The support effect on structure sensitivity of cobalt-based Fischer-Tropsch synthesis

de Laat, Michelle E.

Award date:
2021

Department of Chemical Engineering and Chemistry
Inorganic Materials and Catalysis

The support effect on structure sensitivity of cobalt-based Fischer-Tropsch synthesis

Master Thesis

M.E. de Laat

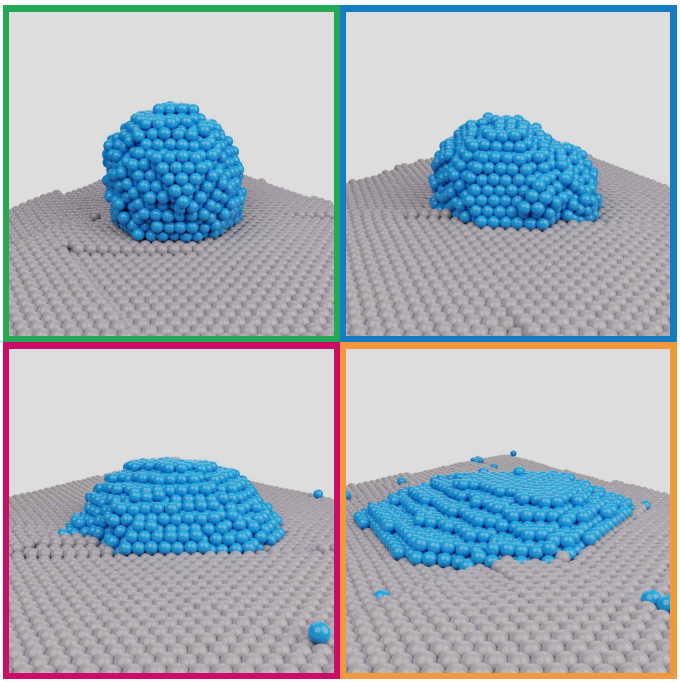

Graduation Committee:
Prof. dr. ir. E.J.M. Hensen
Dr. ir. I.A.W. Filot
Dr. A. Forner Cuenca
Ir. M.P.C. van Etten

Eindhoven, June 2020

Abstract

Different experimental studies show that wetting effects, due to the metal-support interaction, have a profound effect on the activity and selectivity in heterogeneous catalysis. The exact mechanism by which these effects propagate from the nanoscale to the mesoscale is however not yet fully understood. It can be hypothesized that strong metal-support interactions change the curvature of the surface layer, by which particular crystal facets become more favourable over those as commonly predicted by e.g. a Wulff construction. As the topology of the facets enclosing the catalytic nanoparticle determines the surface density of specific active sites, it is reasonable to anticipate that metal-support interactions can play an important role in the performance of the catalyst.

To study the synergistic mechanism by which local metal-support interactions evolve to the observed activity and selectivity patterns, we have developed a novel modelling approach wherein we extend an existing ReaxFF potential that describes Co-Co interactions by a description of the interaction with a fictitious support material. Despite that this material is fictitious in the sense that it is not a realistic catalyst support material such as alumina or silica, it has the strong advantage that we can tune the interaction strength via a single parameter in the model or change the topology of the support by fixating the geometry of the support.

Using the Co/Support potential, we have performed a series of simulated annealing experiments with varying particle sizes in the range of 2-9 nm. Furthermore, we modified the value for the metal-support interaction parameter in such a way that we explored a broad range of conditions varying between strong wetting to strong dewetting conditions.

Performing these annealing simulations with different particle sizes has given more insight in the effect of the interaction between the metal and the support on the different active sites. By identifying the different sites, using a pattern recognition algorithm based on CNA, the surface site fractions have been determined for the different metal-support interaction strengths and particle sizes.

We have showed that the FCC(110)-oriented step-edge site has the highest contribution to the total activity of the nanoparticles, coherent with experimental observations. Therefore, it is expected that the FCC(110)-oriented step-edge site is most likely accounting for the activity of the cobalt-based Fischer-Tropsch synthesis.

Contents

Chapter 1

Introduction

The world is still heavily reliant on fossil fuels, yet is slowly shifting towards renewable energy sources as can be seen from Figure 1.1. However, the pace of shifting towards renewable energies is not fast enough to cope with the growing population and the economic expansion. As can be seen in Figure 1.1, it is expected that the world is still mostly depending on fossil fuels like coal, natural gas and oil for the next decades. However, the fossil fuel reserves are depleting [1].
As fuel consumption from the transport sector comprises a sizeable portion of total fossil fuel consumption [2], alternative processes to produce longer hydrocarbons have to be utilized. The Fischer-Tropsch synthesis is an interesting technology to obtain longer hydrocarbons as the feed stock can be derived from alternative sources such as coal, natural gas, CO_2 and biomass. Especially, when synthesis gas can be obtained from CO_2 or biomass, an important step towards sustainability can be made. The Fischer-Tropsch synthesis converts synthesis gas ($CO + H_2$) into longer hydrocarbons, wherein, catalysts play an import role, to reduce the energy requirements for this process. To better understand the Fischer-Tropsch synthesis, the role of catalysis will be explained first.

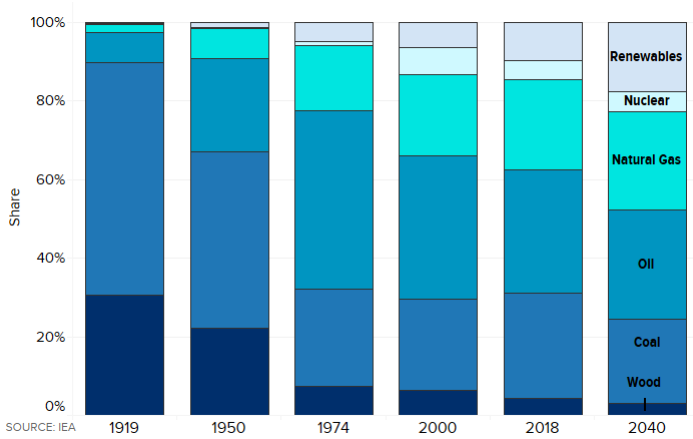

Figure 1.1: Share of resources to meet the global energy demand from 1919 to 2040 [3].

1.1 Catalysis

The straightforward explanation of a catalyst is that a catalyst accelerates a chemical reaction, but is not consumed. A catalysts can improve the conversion, saves energy, can convert undesired byproducts into harmless molecules and can improve selectivity so less waste products are formed. Figure 1.2 shows the cycle of a catalytic reaction, wherein first the molecules bond to the catalyst (adsorption), then the reaction occurs. If the product is formed, it will be released from the catalyst so a new reaction can take place (desorption). The catalyst offers an alternative path for the reaction, which is kinetically more favorable than the non-catalytic pathway. Therefore, milder operating conditions such as lower temperature and pressure can be used.

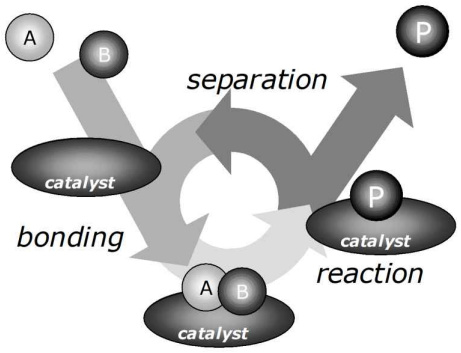

Figure 1.2: Catalytic reaction cycle [4].

Within the field of catalysis, a distinction can be made between three types of catalysts: homogeneous, heterogeneous and bio catalysts. In homogeneous catalysis, the substrates for a reaction and the catalyst are brought together in one phase. Typically, the reagents and catalyst are both in the liquid phase, but can also be in the gas phase [5]. In heterogeneous catalysis, catalysts are solids which catalyze a reaction of molecules in the gas or liquid phase. The catalytic reaction occurs on the surface of the catalyst. In bio catalysis, enzymes are used as catalyst. The enzyme is a large protein with an active site in a specific shape formed by the protein structure. These specific shapes ensure that bio-catalysts are highly selective and efficient catalysts.

1.2 Fischer-Tropsch synthesis

The Fischer-Tropsch process is developed in 1923 by two German scientists, Franz Fischer and Hans Tropsch at the Kaiser-Wilhelm-Institut für Kohlenforschung in Mülheim an der Ruhr. [4]. In the Fischer-Tropsch process, synthesis gas, which is a mixture of CO and H_2, is converted into a wide range of hydrocarbons, oxygenates and water. Equation 1.1 shows the overall reaction of the Fischer-Tropsch synthesis. Synthesis gas can be derived from fossil fuels such as oil, natural gas, coal, or from more renewable sources such as CO_2 and biomass.

$$(2n+1)H_2 + nCO \rightleftarrows C_nH_{(2n+2)} + nH_2O \tag{1.1}$$

The Fischer-Tropsch synthesis contains three steps for the polymerization reaction, namely, an initiation, several propagation steps and a termination step. The most likely mechanism for the Fischer-Tropsch chain growth is the carbide mechanism. In the carbide mechanism the CO is adsorbed onto the surface first, subsequently, the carbon dissociates and hydrogenates resulting in CH_x intermediates. The CH_x can be inserted in another hydrocarbon chain, resulting in a longer hydrocarbon chain. The chain growth can continue or the chain growth can be terminated by hydrogenation into an alkane or alkene. Finally, the formed hydrocarbon desorbs from the surface and the oxygen is removed from the surface as water, as the result of two hydrogenation steps. For the Fischer-Tropsch synthesis several transition metals can be used as catalysts, showed in Figure 1.3. However, not all transition metals result in the same selectivity towards the desired end products. For palladium, osmium, iridium and platinum the dissociation of CO is more difficult. Therefore, the CO is hydrogenated to form methanol which is undesirable. Rhodium has a moderate dissociation rate of CO dissociation and a relatively slow methane formation rate, which results in longer oxygenates. To have a high rate of CO dissociation it is possible to use the four metals cobalt, iron, nickel and ruthenium. However, the CO dissociation for nickel is much slower compared to the methane formation rate. Cobalt, iron and ruthenium all have a high CO dissociation and CH_x formation rate to produce longer hydrocarbon chains [6]. The high price of ruthenium makes this catalyst not suitable for large scale operations. Both iron and cobalt can be used for large scale application as they are cheaper [7]. Iron catalysts are even less expensive than cobalt catalysts, however, iron catalysts are also less stable in the conditions present in Fischer-Tropsch synthesis [4]. Within this thesis the focus will be on the cobalt-based Fischer-Tropsch synthesis.

Figure 1.3: Fischer-Tropsch product selectivity for different transition metals [6].

1.3 Structure sensitivity in cobalt-based Fischer-Tropsch synthesis

Experimental research has shown that the turnover frequency of a cobalt catalyst improves until its particle size reaches approximately 6 nm [8][9][10]. It is therefore hypothesized that the facets forming the active sites of the catalyst follow a similar trend as the experimentally obtained structure sensitivity trend. Research performed by van Etten et al. [11] shows the distribution of different facets for differently sized cobalt nanoparticles, see Figure 1.4. It can be seen from Figure 1.4 that the FCC(111) and FCC(100)-oriented terrace sites and FCC(211) and FCC(110)-oriented step-edge sites follow a similar trend as the experimentally obtained structure sensitivity trend. Therefore, it is expected that these facets form the active sites of the catalyst. However, this study was performed on unsupported cobalt nanoparticles. This is in contrast with experimental studies as they do include a support material.

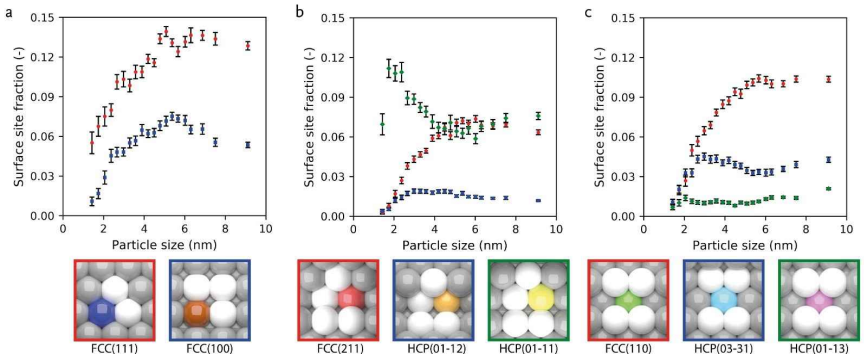

Figure 1.4: Abundance of terrace sites (a) and step-edge sites (b, c) as function of particle size. a, (red) threefold sites with FCC(111) orientation and (blue) fourfold sites with FCC(100) orientation. b, five-fold sites of orientations (red) FCC(211), (blue) HCP(01-12) and (green) HCP(01-11). c, five-fold sites with orientations (red) FCC(110), (blue) HCP(03-31) and (green) HCP(01-13). Error bars correspond to the 95% confidence intervals determined by averaging over 40 simulations of particles of the same size. This figure is taken from the work of van Etten et al. [11].

Different experimental studies show that wetting effects, due to the metal-support interaction, have a profound effect on activity and selectivity in heterogeneous catalysis. However, the exact mechanism by which these effects propagate from nanoscale to mesoscale is not yet fully understood [12][13][14]. It can be hypothesized that strong metal-support interactions change the curvature of the surface layer, by which particular crystal facets become more favorable over those as commonly predicted by e.g. a Wulff construction. As the topology of the facets enclosing the catalytic nanoparticle determines the surface density of specific active sites, it is reasonable to anticipate that metal-support interactions may play an important role in the performance of the catalyst. Therefore, in the present work structure sensitivity trends of cobalt-based Fischer-Tropsch synthesis in the presence of a support will be investigated.

1.4 The scope of this thesis

The goal of this work is to unravel the support effect on the structure sensitivity of cobalt-based Fischer-Tropsch synthesis. First, the synergistic mechanism by which local metal-support interactions evolve has to be studied. In order to perform molecular dynamics simulations for constructing supported cobalt nanoparticles, first a force field has to be constructed which describes both the catalytic material and the support material, as well as the cobalt/support interaction.

Using the metal-support potential, a series of simulated annealing experiments will be performed with varying particle size in the range of 2-9 nm. These simulated annealing calculations will be performed over a broad range of metal-support interactions strengths varying from strong wetting to strong dewetting conditions.

From these simulated annealing calculations, more insight can be obtained about the dependency of the nanoparticle activity on the particle size and metal-support interaction strength. Firstly, the different active sites are identified using a pattern recognition algorithm based on CNA [15]. By coupling the obtained site fractions as function of particle size and metal-support interactions, structure sensitivity trends for supported cobalt nanoparticles under different wetting conditions can be obtained. From this information, the effect of support on cobalt-based Fischer-Tropsch synthesis and can be elucidated.

Chapter 2

Method

2.1 Reactive Force Field

For modeling metal/support systems for particle sizes in the range of 2-9 nm, the number of atoms in the system will vary between around 1.000 to 100.000 atoms. Therefore, these metal/support systems cannot be studied using state-of-the-art Density Functional Theory (DFT). In order to model these systems, Molecular Dynamics simulations will be performed using a force field (ReaxFF), based on an extensive set of structural and energetic data from first-principles calculations based on spin-polarized DFT calculations. To describe a system, around 100 variables per element needs to be defined and fitted to the structural and energetic data obtained from DFT calculations. An overview of the different variables can be found in Appendix A. For additional information about the force field and its parameters, the reader is referred to van Duin et al. [16]. Within ReaxFF, the system energy is divided into contributions of various partial energies. Equation 2.1 shows the partial energy contributions of the total energy to the system.

$$E_{\text{system}} = E_{\text{bond}} + E_{\text{over}} + E_{\text{under}} + E_{\text{val}} + E_{\text{pen}} + E_{\text{tors}} + E_{\text{conj}} + E_{\text{vdWaals}} + E_{\text{Coulomb}} \tag{2.1}$$

Within Equation 2.1 E_{bond} represents the bond energy, E_{over} and E_{under} represent energy due to the over and under coordination respectively, E_{val} represents the valance angle energy, E_{pen} is a penalty energy for stabilizing the three-body system with a center atom which contains two double bonds connected to it, E_{tors} represents the torsion angle energy, E_{conj} represents the conjugated system energy, E_{vdWaals} represents the non-bonded van der Waals interaction energy and E_{Coulomb} represents the coulomb interaction energy [16][17][18].

The ReaxFF method is based on the relationship between a bond order and bond distance. The bond order $\text{BO}_{ij}{}'$ between a pair of atoms can be calculated via Equation 2.2. However, the assumption was made that the bond order can directly be obtained from the interatomic distance r_{ij}. Equation 2.2 consists of three exponential terms which correspond to the contribution of the sigma, the first pi and the second pi bond, respectively [16][18].

$$\text{BO}'_{ij} = \exp\left[p_{\text{bo},1} \cdot \left(\frac{r_{ij}}{r_0}\right)^{p_{\text{bo},2}}\right] + \exp\left[p_{\text{bo},3} \cdot \left(\frac{r^{\pi}_{ij}}{r_0}\right)^{p_{\text{bo},4}}\right] + \exp\left[p_{\text{bo},5} \cdot \left(\frac{r^{\pi\pi}_{ij}}{r_0}\right)^{p_{\text{bo},6}}\right] \tag{2.2}$$

2.2 Simulated annealing

In simulated annealing calculations the particles are brought to a high temperature, to be able to move out of their initial lattice. Subsequently, the system is slowly cooled down via the Molecular Dynamics simulated annealing procedure. If the temperature is decreased on a logarithm scale compared to time, a potential-energy minimum can be obtained by the system [19][20]. The program ADF2019.104 is used to perform the simulated annealing calculations.

Using simulated annealing, cobalt nanoparticles on a support have been constructed with Molecular Dynamics. The initial temperature for the simulated annealing calculations is 1500 K. To control the temperature during the simulated annealing calculations a Nosé-Hoover chains thermostat was used, with a temperature damping constant of 100 fs. For the Molecular dynamic simulations a velocity Verlet algorithm is used with a time step of 0.25 fs in the canonical ensemble (NVT). The atomic charges are calculated using the Electron Equilibrium Method (EEM) approach [16].

The number of iterations during initialization is dependent on the amount of atoms present in the system. For most of the simulated annealing calculations the number of iteration steps during initialization is 400.000 time steps of 0.25 fs and the system was cooled down from 1500 K to 300 K with 40.000 iterations per annealing step of 100 K. The simulated annealing simulations will take a lot of computational time to obtain the potential-energy minimum. Therefore, the amount of support atoms is minimized without influencing the final result of the simulated annealing calculations. Also a high enough initial temperature is required in order to initialize the the system. However, a not completely initialized system can be the result of a low initial temperature. Finally, a low number of iterations steps is required, however, the number of iteration steps need to be high enough to obtain the potential-energy minimum. These simulated annealing settings will be elaborated on in Chapter 3.3.

2.3 Site Recognition

After the simulated annealing calculations, the different sites on the surface of the cobalt nanoparticle have to be identified. The different sites will be identified using a pattern recognition algorithm based on the common neighbour analysis (CNA) method [15]. The CNA method identifies a signature for each particle by evaluating the topology of the neighbourhood particles of that specific particle. The neighbourhood is defined by using a cutoff radius. The cutoff radius $r_{\text{cut}}(i)$ of particle i is calculated via Equation 2.3, where $\vec{r}_{ij}$ is the displacement vector between particles i and j. Subsequently, a list of neighbour particles is generated which lie in the cutoff radius range. An adjacency matrix is generated of the neighbourhood particles, omitting the central particle. The adjacency matrix is a binary matrix in which a zero indicates that a particle does not lie within the cutoff radius of another particle and a one indicates that a particle does lie within the cutoff radius of another particle. The next step is to generate a neighborhood graph. For each of the particles in the graph, three characteristic indices are calculated, omitting the central particle. The indices *i*,*j* and *k* represent the number of adjacent particles, number of edges between the those particle and the longest path among only those edges respectively. To assign a CNA signature, the indices (*i*,*j*,*k*) of all neighbourhood particles of the central particle are collected.

$$r_{\text{cut}}(i) = \left(\frac{1+\sqrt{2}}{2}\right)\left(\frac{1}{6}\sum_{j=1}^{6}|\vec{r}_{ij}|\right) \tag{2.3}$$

Figure 2.1 present the schematic illustration of the CNA calculation for a central particle 0. The cutoff radius, described via Equation 2.3, is applied for particle 0, which resulted in a neighbourhood of particles 1 until 9 (I). The adjacency matrix is created by evaluating Equation 2.3 for each of the neighbourhood particles (II). In Figure 2.1 it can be seen that particle 3 (presented in orange) has three neighbour particles, namely, particle 2, 4 and 8. Particle 9 (presented in blue) has 4 neighbour particles, namely, particle 5, 6, 7 and 8. Subsequently, a neighbourhood graph is generated (III). For particle 3, it can be seen that it has three adjacency neighbours (*i*), represented by the orange striped nodes. The orange dashed lines represent the edge connecting the adjacent particles in the neighbourhood of particle 3. Therefore, the indices *j* of particle 3 is assigned with a one. The continuous orange line represents the longest path among the edges *k*. In the case of particle 3, the longest path between the edges is one. The indices for particle 3 therefore, are (3,1,1). For particle 9 the indices (4,2,1) are obtained via the same method as particle 3 however, this is visualized in blue. It can be seen that particle 9 has 2 edges between particles in the neighbourhood and the longest path between the edges is one. After obtaining all indices of the different particles in the neighbourhood of particle 0, a CNA signature can be obtained (IV). Particles 1, 2, 3, 5 and 6 all have the same indices as particle 3 (3,1,1) and particles 7 and 8 have the same indices as particle 9. Therefore, the CNA signature for particle 0 is equal to {6 × (3,1,1), 3 × (4,2,1)}.

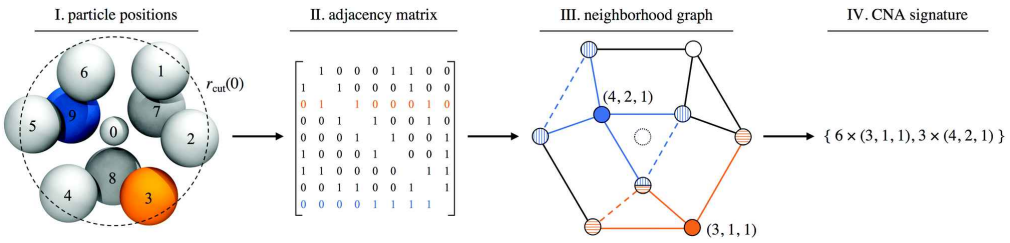

Figure 2.1: Schematic illustration of the CNA calculation for the FCC(111) face [15].

In this thesis, this algorithm is used to determine the CNA signatures of all atoms in the system. However, as the surface sites on the cobalt nanoparticle are of interest, the CNA signatures of just the cobalt atoms are taken into account for calculating the surface site fractions.

Chapter 3

Results & Discussion

To elucidate the influence of the metal-support interaction strength on the structure sensitivity of cobalt-based Fischer-Tropsch synthesis, simulated annealing calculations have been performed. In this chapter the results of these simulations will be discussed. In order to study the metal-support interactions, first the initialization of the coordinates of both the metal and support atoms will be determined. Subsequently, the implementation of different metal-support interactions for the simulated annealing calculations will be explained. In addition, settings such as support size, initial temperature and the number of iterations needed to be determined. When these settings were determined, simulations were performed for a range of particle sizes and metal-support interaction strengths. Finally, structure sensitivity trends for each of the simulated metal-support interactions were obtained by linking the obtained size-dependent surface site fractions with the corresponding activities.

3.1 Initial coordinates

To perform the simulated annealing calculations, the initial positions of the metal and support atoms have to be determined. A script was developed in order to generate the initial positions for each of the metal and support atoms. The cobalt atoms are initially positioned on a simple cubic lattice. This is done in such a way that all atoms have the same distance between its direct neighbouring atoms. This cube of metal atoms is placed centrally on top of the layers of support atoms. For the support, an FCC(111) structure is chosen since this structure is present in the FCC crystal as well as the HCP crystal structure. Therefore, it is expected that no bias towards a specific bulk or surface structure is generated. The FCC(111) support contains four layers of atoms. It is desired to have a low influence of the shape of the support, since any roughness may also have an influence on the shape of the particle. However, researching the influence of roughness on the shape of the particle is outside of the scope of this thesis. Figure 3.1 shows the initial positions of the FCC(111) support with the cobalt particle cube of $12 \times 12 \times 12$ cobalt atoms placed centrally on top of it.

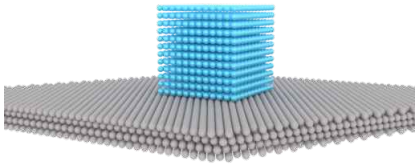

Figure 3.1: Initial position of 12 × 12 × 12 cobalt atoms on a FCC(111) support.

For each combination of particle size and metal-support interaction strength, 40 simulations were performed for statistical averaging. A random velocity was assigned to each of the atoms in the system (both metal and support atoms) according to a Gaussian distribution. The random initial velocities are scaled to the initial temperature of the system (1500 K). The Mersenne Twister generator is used to generate random numbers [21].

3.2 Force Field

The in-house trained force field for cobalt [17] is used as a starting point for a force field, describing both the cobalt-cobalt interaction as well as the cobalt-support interactions. As a first attempt to model support-metal systems on the basis of a force field, a fictitious support was used. This means that both the atomic and two-body parameters for cobalt were used as a basis for the atomic and two-body parameters describing the support material. Only one parameter was adjusted in the atomic parameter set for the support, namely the atomic mass. The atomic mass was drastically increased in order to prevent movement of support atoms as much as possible. A complete overview of the force field describing cobalt/support systems can be found in Appendix B. Despite that the support material is fictitious in a sense that it is not a realistic catalyst support material such as alumina or silica, it has the strong advantage that the metal-support interaction strength can be tuned with only one single parameter.

Equation 3.1 shows the partial energy contribution of the bond energy to the energy of the system in ReaxFF. By changing the bond energy, the metal-support interaction strength can be tuned. Therefore, only a single parameter has to be tuned from Equation 3.1. By changing the dissociation energy (D_e), the bond energy of the metal-support interaction can be tuned.

$$E_{\text{bond}} = -D_e \cdot \text{BO}_{ij} \cdot \exp[p_{\text{be},1}(1 - \text{BO}_{ij}^{p_{\text{be},1}})] \tag{3.1}$$

The initial value of the dissociation energy is 53.5381 kcal/mol. To tune metal-support interactions this value will be changed. Appendix A1 shows the force field of the lowest metal-support interaction, which is 35 kcal/mol. The reason for choosing 35 kcal/mol as the lower boundary in our simulations is that too weak metal-support interactions will result in spherical cobalt nanoparticles floating above the support. Increasing the value above 55 kcal/mol will lead to a cluster of metal and support atoms. Therefore, metal-support interaction strengths of 35, 40, 45 and 50 kcal/mol are used for the simulations. To obtain a clear overview of all results, a color scheme is used for the different metal-support interaction strengths throughout this thesis. The colors which are used are green, blue, pink and orange, as shown in Figure 3.2, in which green and orange are the weakest and strongest metal-support interactions, respectively.

Figure 3.2: Color scheme for the different metal-support interactions. Green represents D_e = 35 kcal/mol, blue represents D_e = 40 kcal/mol, pink represents D_e = 45 kcal/mol and orange represents D_e = 50 kcal/mol.

3.3 Simulated annealing settings

Performing annealing simulations can result in high computational costs, especially when a high number of atoms is used. In this chapter three different parameters will be investigated to reduce the computational time for the annealing simulations: (1) support size, (2) the initial temperature, and (3) the number of iteration time steps.

3.3.1 The size of the metal-support

To decrease the computational time, the number of atoms used in the annealing simulations need to be limited. The amount of support atoms will have a high influence on the simulation time. Since the particle size increases with increasing metal-support interaction strength, the minimum support size will be determined by the strongest metal-support interaction strength (D_e = 50 kcal/mol). The support has to be large enough for all the molecules to fit onto the support when the metal-support interaction strength is strong. This is due to the better wetting of the metal onto the support when the interaction strength is strong. Initially, a simple cubic cobalt particle is placed on top of the support. The simple cubic consists of $12 \times 12 \times 12$ cobalt atoms in the x, y and z-direction. The support size is determined by the amount of cobalt atoms in the x, y and z-direction. The support is chosen to be 3, 4, 5 and 6 times the amount of cobalt atoms in the x and y-direction and consists of four layers. This results in a total of 5.184, 9.216, 14.400 and 20.736 support atoms, respectively, for a cobalt particle consisting of 1728 atoms ($12 \times 12 \times 12$). Figure 3.3 shows the initial positions of the cobalt atoms on the different sizes of support.

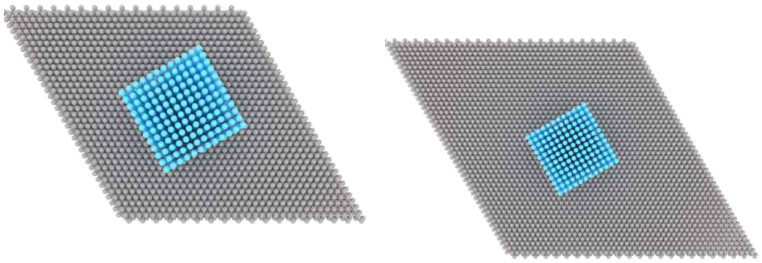

(a) Support of 5.184 atoms (36 × 36 × 4).

(b) Support of 9.216 atoms (48 × 48 × 4).

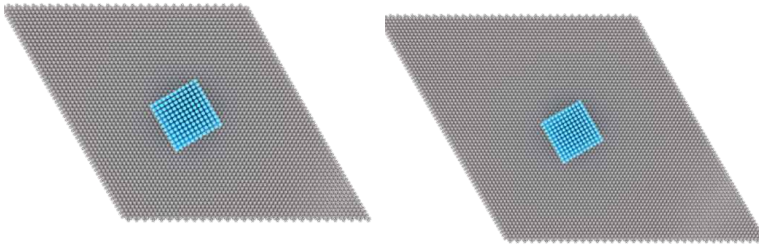

(c) Support of 14.400 atoms (60 × 60 × 4).

(d) Support of 20.736 atoms (72 × 72 × 4).

Figure 3.3: Initial positions of the cobalt particle on a FCC(111) support with different support sizes.

The annealing simulation will start at an initial temperature of 1500 K and will slowly decrease to 300 K. The number of iterations steps during the initialization will be set to 400.000 and the iterations per annealing step of 100 K will be set at 40.0000. This will be kept constant for all different support sizes.

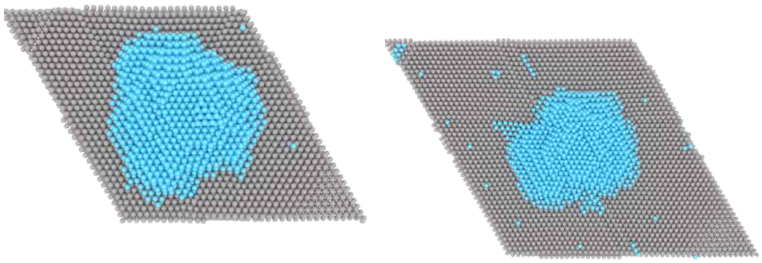

(a) Support of 5.184 atoms (36 × 36 × 4).

(b) Support of 9.216 atoms (48 × 48 × 4).

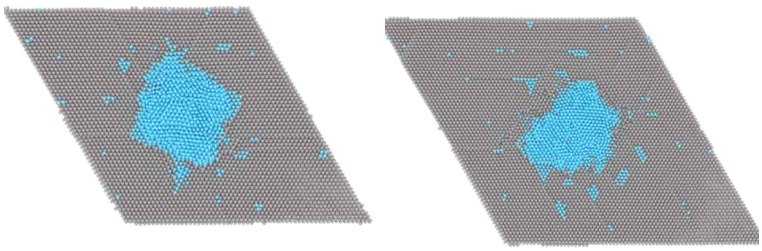

(c) Support of 14.400 atoms (60 × 60 × 4).

(d) Support of 20.736 atoms (72 × 72 × 4).

Figure 3.4: Final positions of the cobalt particle on a FCC(111) support with different support size and a strong metal-support interaction strength.

Figure 3.4, shows the positions of the cobalt atoms after the annealing simulation. In Figure 3.4a, it can be seen that for a support size 3 times larger than the amount of cobalt particles, the support is not large enough. The cobalt particles are close to the edge of the support and therefore a larger support would be desired. As can be seen in Figure 3.4b, 3.4c and 3.4d with a support size 4, 5 and 6 times the number of cobalt atoms in the x and y-direction the support surface is large enough. For all different sizes, the cobalt atoms are not close to the edges of the support. Therefore, to reduce the computational time a support size of 4 times the atoms of a cobalt particle in the x and y-direction is chosen for the annealing simulations.

3.3.2 The initial annealing temperature

Simulated annealing calculations were performed to investigate the influence of the initial temperature on the wetting effect of the cobalt particle. These simulations have also been performed to lower the initial temperature as much as possible. A lower initial temperature results in less computational time needed for the simulated annealing calculations as the total cooling trajectory will be shorter when the initial temperature is lower. Different initial temperatures in a range of 800 K until 1500 K where used to investigate which initial temperature is desired for the simulated annealing calculations. The simulated annealing calculations will be performed with different metal-support interaction strengths. The simulated annealing calculations will start at the different initial temperatures and will slowly decrease until 300 K. A support size of 4 times the atoms of a cobalt particle in the x and y- direction will be used. The number of iteration steps during the initialisation will be set at 400.000 and the iterations per annealing step will be set at 40.0000. This will be kept constant for all different initial temperatures, as the number of atoms does not change.

Figures 3.5-3.8 represent the results of the different initial temperatures with different metal-support interaction strengths. As can be seen in Figures 3.5-3.8 there is a slight difference between the initial temperatures on the final positions of the cobalt atoms. With an increasing initial temperature, the support atoms will have more energy to move, which is not desired.

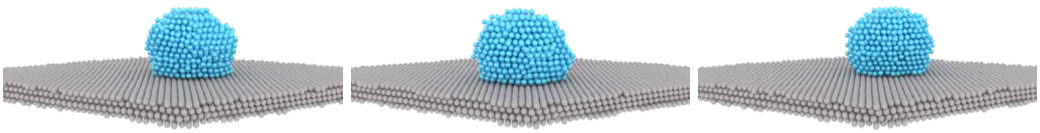

(a) Initial temperature of 800 K. (b) Initial temperature of 900 K. (c) Initial temperature of 1000 K.

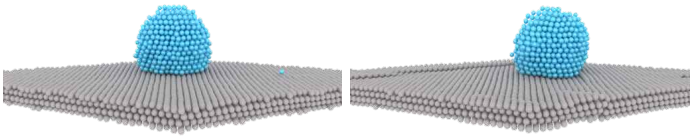

(d) Initial temperature of 1100 K. (e) Initial temperature of 1500 K.

Figure 3.5: Final positions of the cobalt particle on a FCC(111) support with different initial temperatures and a weak metal-support interaction strength (D_e = 35 kcal/mol).

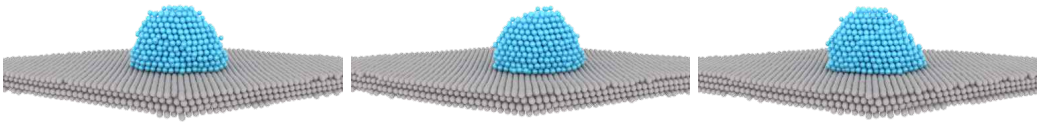

(a) Initial temperature of 800 K. (b) Initial temperature of 900 K. (c) Initial temperature of 1000 K.

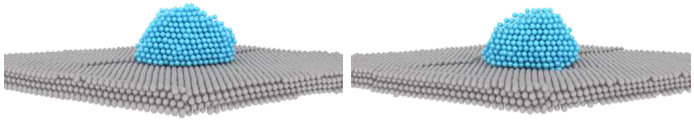

(d) Initial temperature of 1100 K. (e) Initial temperature of 1500 K.

Figure 3.6: Final positions of the cobalt particle on a FCC(111) support with different initial temperatures and a moderate metal-support interaction strength (D_e = 40 kcal/mol).

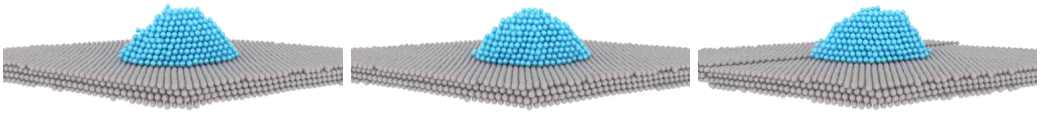

(a) Initial temperature of 800 K. (b) Initial temperature of 900 K. (c) Initial temperature of 1000 K.

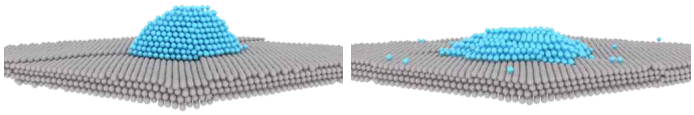

(d) Initial temperature of 1100 K. (e) Initial temperature of 1500 K.

Figure 3.7: Final positions of the cobalt particle on a FCC(111) support with different initial temperatures and a moderate metal-support interaction strength (D_e = 45 kcal/mol).

(a) Initial temperature of 800 K. (b) Initial temperature of 900 K. (c) Initial temperature of 1000 K.

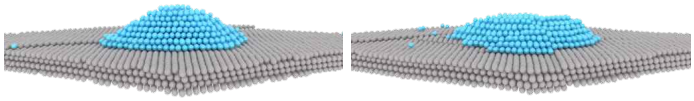

(d) Initial temperature of 1100 K. (e) Initial temperature of 1500 K.

Figure 3.8: Final positions of the cobalt particle on a FCC(111) support with different initial temperatures and a strong metal-support interaction strength (D_e = 50 kcal/mol).

Based on the visualisation of the formed cobalt nanoparticles alone, it is difficult to make a decision about which initial temperature should be used. To quantify these results, the number of unknown surface sites have to be identified, using the pattern recognition algorithm. As described in Chapter 2.3 the program recognises different particle signatures. The unknown surface sites are sites which are not recognized by the pattern recognition algorithm. There are two possible explanations as to why these sites are not recognized. First, the site could be at the edge or corner of the nanoparticle of which the CNA signature is not known. The second explanation is that the surface sites are not perfectly formed crystal structures (amorphous structures). A side note to this, is that the surface site fraction of the unknown sites is on the basis of the surface atoms only. Figure 3.9 shows the percentage of unknown sites at the different initial temperatures. It can be seen that with a higher initial temperature, less unknown sites are observed for all different metal-support interaction strengths. Therefore, the initial temperature of 1500 K will be used for the simulated annealing calculations.

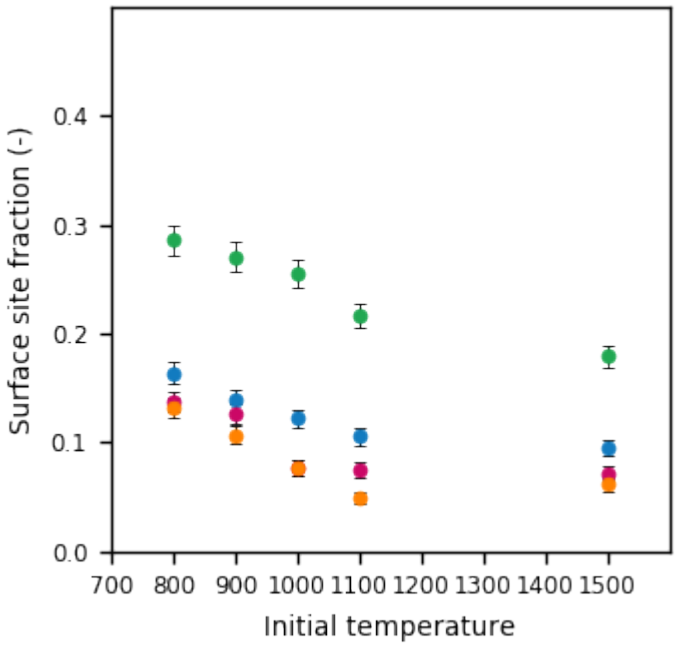

Figure 3.9: Unknown surface site fraction by different initial temperature and for different metal-support interaction strengths. Note that green, blue, pink and orange represent the different metal-support interaction strengths from weak to strong, respectively.

3.3.3 The number of initial initialisation steps

The number of iteration steps is important since a large number of iteration steps will increase the computational time. However, the number of iteration steps need to be large enough for the particles to have enough time to form a final bulk structure. Therefore, it will be investigated which number of iteration steps is preferred for the simulated annealing calculations with different metal-support interaction strengths. The simulated annealing calculations will start at a temperature of 1500K. The number of iteration steps during initialization will be varied from 1.000 until 400.000. Table 3.1 shows the different number of iterations during initialization and the number of iterations per annealing step.

Table 3.1: Overview of the different iterations during initialization and the number of iterations per annealing step.

Iterations during initialization	Iterations per annealing step
1.000	100
5.000	500
10.000	1.000
50.000	5.000
100.000	10.000
150.000	15.000
200.000	20.000
300.000	30.000
400.000	40.000

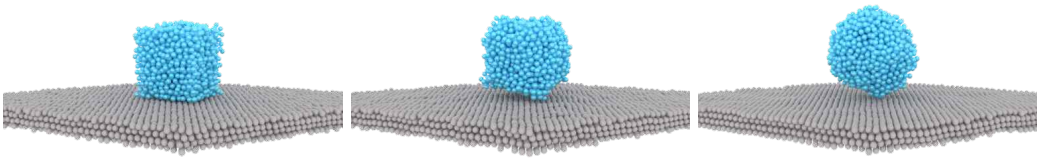

(a) 1.000 iteration steps during initialization and 100 iterations per annealing step.

(b) 5.000 iteration steps during initialization and 500 iterations per annealing step.

(c) 10.000 iteration steps during initialization and 1.000 iterations per annealing step.

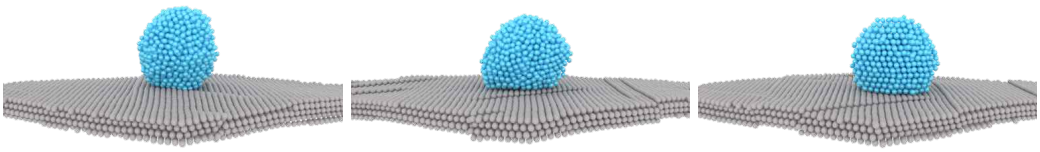

(d) 50.000 iteration steps during initialization and 5.000 iterations per annealing step.

(e) 100.000 iteration steps during initialization and 10.000 iterations per annealing step.

(f) 150.000 iteration steps during initialization and 15.000 iterations per annealing step.

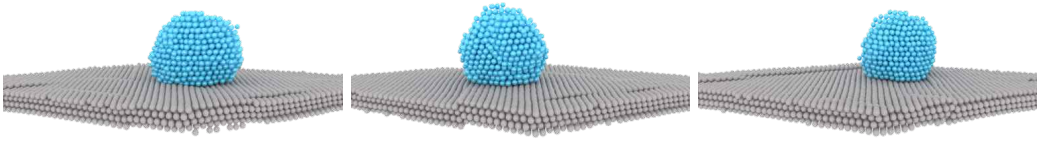

(g) 200.000 iteration steps during initialization and 20.000 iterations per annealing step.

(h) 300.000 iteration steps during initialization and 30.000 iterations per annealing step.

(i) 400.000 iteration steps during initialization and 40.000 iterations per annealing step.

Figure 3.10: Final positions of the cobalt particle on a FCC(111) support with a weak metal-support interaction strength (D_e = 35 kcal/mol) and a different number of iterations during initialization and iteration steps.

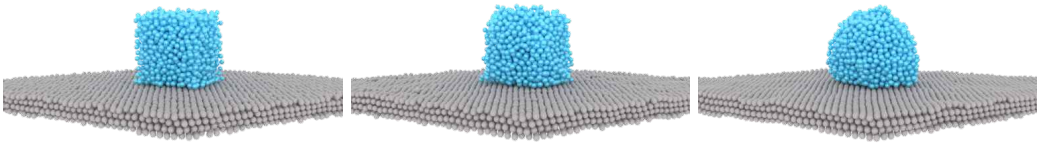

(a) 1.000 iteration steps during initialization and 100 iterations per annealing step.

(b) 5.000 iteration steps during initialization and 500 iterations per annealing step.

(c) 10.000 iteration steps during initialization and 1.000 iterations per annealing step.

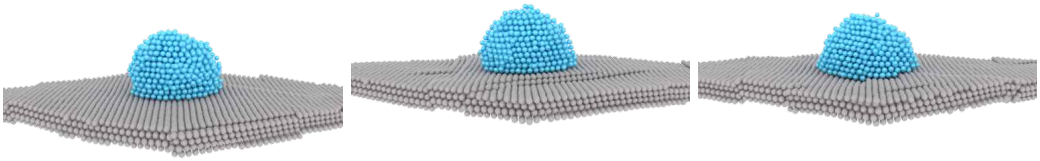

(d) 50.000 iteration steps during initialization and 5.000 iterations per annealing step.

(e) 100.000 iteration steps during initialization and 10.000 iterations per annealing step.

(f) 150.000 iteration steps during initialization and 15.000 iterations per annealing step.

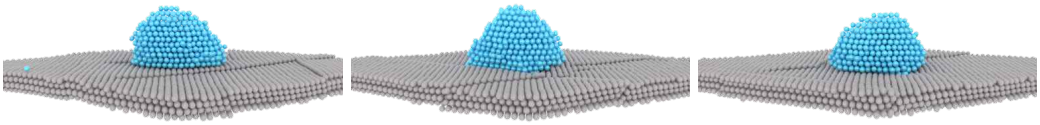

(g) 200.000 iteration steps during initialization and 20.000 iterations per annealing step.

(h) 300.000 iteration steps during initialization and 30.000 iterations per annealing step.

(i) 400.000 iteration steps during initialization and 40.000 iterations per annealing step.

Figure 3.11: Final positions of the cobalt particle on a FCC(111) support with a moderate metal-support interaction strength (D_e = 40 kcal/mol) and a different number of iterations during initialization and iteration steps.

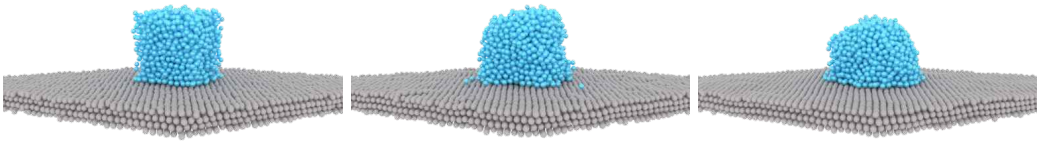

(a) 1.000 iteration steps during initialization and 100 iterations per annealing step.

(b) 5.000 iteration steps during initialization and 500 iterations per annealing step.

(c) 10.000 iteration steps during initialization and 1.000 iterations per annealing step.

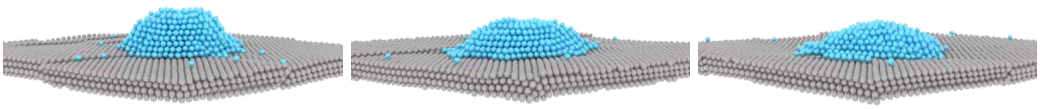

(d) 50.000 iteration steps during initialization and 5.000 iterations per annealing step.

(e) 100.000 iteration steps during initialization and 10.000 iterations per annealing step.

(f) 150.000 iteration steps during initialization and 15.000 iterations per annealing step.

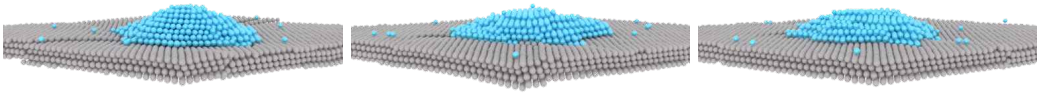

(g) 200.000 iteration steps during initialization and 20.000 iterations per annealing step.

(h) 300.000 iteration steps during initialization and 30.000 iterations per annealing step.

(i) 400.000 iteration steps during initialization and 40.000 iterations per annealing step.

Figure 3.12: Final positions of the cobalt particle on a FCC(111) support with a moderate metal-support interaction strength (D_e = 45 kcal/mol) and a different number of iterations during initialization and iteration steps.

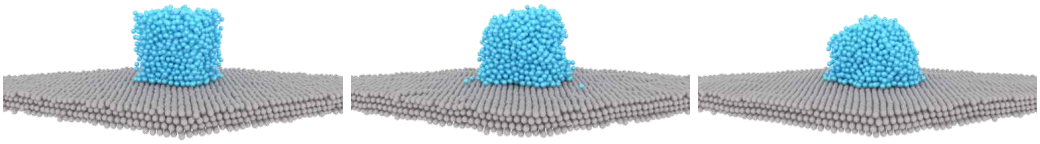

(a) 1.000 iteration steps during initialization and 100 iterations per annealing step.

(b) 5.000 iteration steps during initialization and 500 iterations per annealing step.

(c) 10.000 iteration steps during initialization and 1.000 iterations per annealing step.

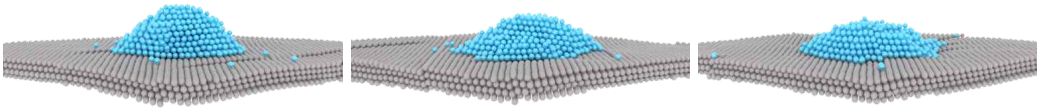

(d) 50.000 iteration steps during initialization and 5.000 iterations per annealing step.

(e) 100.000 iteration steps during initialization and 10.000 iterations per annealing step.

(f) 150.000 iteration steps during initialization and 15.000 iterations per annealing step.

(g) 200.000 iteration steps during initialization and 20.000 iterations per annealing step.

(h) 300.000 iteration steps during initialization and 30.000 iterations per annealing step.

(i) 400.000 iteration steps during initialization and 40.000 iterations per annealing step.

Figure 3.13: Final positions of the cobalt particle on a FCC(111) support with a strong metal-support interaction strength (D_e = 50 kcal/mol) and a different number of iterations during initialization and iteration steps.

From Figures 3.10-3.13, it can be seen that for a small number of iterations during initialization the atoms did not have enough time to move out of their initial lattice. The atoms are almost in the same simple cubic lattice as their initial positions. Figures 3.10-3.13 show, that with increasing the number of iterations during initialization, the atoms are moving out of their initial lattice. A transition can be observed from the initial cubic lattice to a crystalline phase consisting of FCC and HCP-oriented sites. The difference in the final structures of the nanoparticles becomes smaller

after 200.000 iterations during initialization. Therefore, no decision can be made visually. Figure 3.14, presents the surface site fraction of the unknown sites for the different number of iteration steps during initialization. It can be seen that the surface site fraction of unknown sites decreases with increasing number of iterations during initialization. However, for 400.000 iterations during initialisation the surface site fraction for the unknown sites is sufficiently low. However, the surface site fraction of the unknown sites is slightly higher compared to the surface site fraction of the unknown sites of the cobalt nanoparticle in vacuum. This is a result of the atoms at the surface connected to the support, which can't be identified. However, these atoms do not have an influence on the number of active sites, since they are not active.

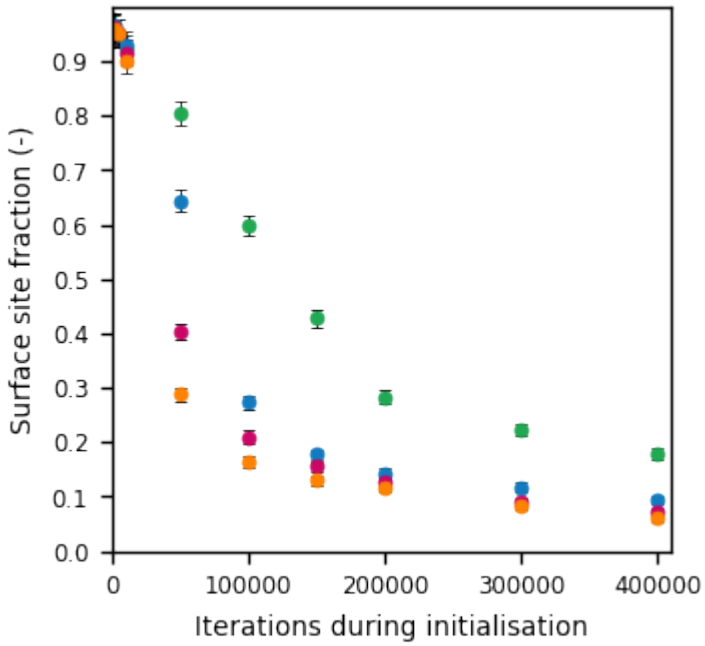

Figure 3.14: Unknown surface site fraction by different number of iterations during initialization and per annealing step for different metal-support interaction strengths. Note that green, blue, pink and orange represent the different metal-support interaction strengths from weak to strong respectively.

To see if the cooling trajectory of the simulated annealing calculations is not too fast the mean square displacement (MSD) will be calculated. With the mean square displacement the degree of fluctuations of the particle positions can be measured. The mean-square displacement is calculated via Equation 3.2 [18].

$$MSD = \frac{1}{N-n} \sum_{i=1}^{N-n} (\vec{r}_{i+n} - \vec{r}_i)^2, \qquad n = 1, ..., N-1 \tag{3.2}$$

In Figures 3.15-3.18, the mean square displacement is presented as function of the simulation time. In Figures 3.15-3.18, the number of molsav is a representation a number of samples taken over a certain time step. For all different simulated annealing calculations with a different number of iteration steps during initialization the same number of samples are obtained. The amount of iteration steps during each time step depends on the total number of iteration steps for the annealing simulations. This results that for all the simulated annealing calculations the systems starts to cool down after 100 samples. As can be seen from Figures 3.15-3.18, for a small number of iterations during initialization the cooling trajectory is too fast. The atoms do not have enough time to form their ordered crystal. It can also be seen that from 300.000 iteration

steps during initialization a plateau can be observed around ∼175 samples. For 400.000 iterations steps during initialization the plateau can be observed around ∼150 samples. This means that nanoparticles with an ordered bulk phase are being formed before the system is completely cooled down. Therefore, the number of iteration steps during initialization will be set at 400.000.

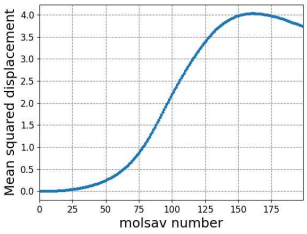

(a) 1.000 iteration steps during initialization and 100 iterations per annealing step.

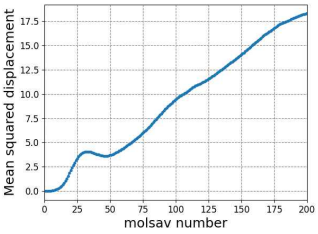

(b) 5.000 iteration steps during initialization and 500 iterations per annealing step.

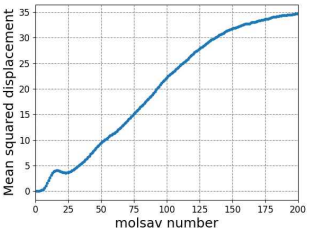

(c) 10.000 iteration steps during initialization and 1.000 iterations per annealing step.

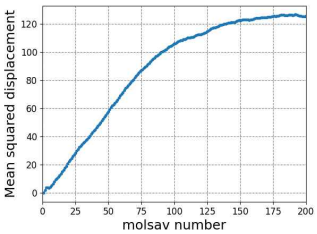

(d) 50.000 iteration steps during initialization and 5.000 iterations per annealing step.

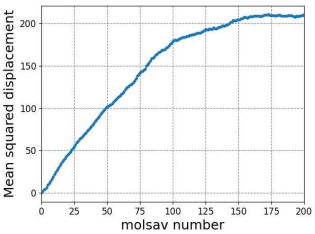

(e) 100.000 iteration steps during initialization and 10.000 iterations per annealing step.

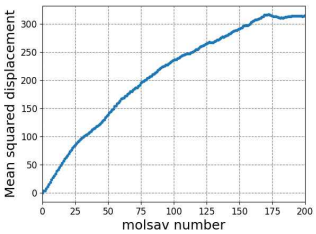

(f) 150.000 iteration steps during initialization and 15.000 iterations per annealing step.

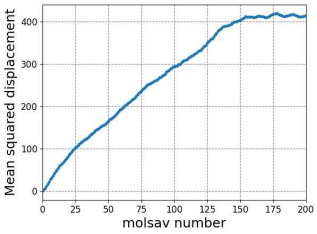

(g) 200.000 iteration steps during initialization and 20.000 iterations per annealing step.

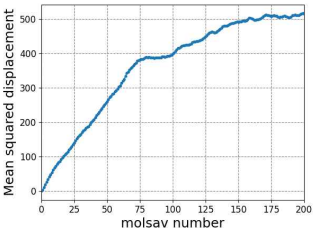

(h) 300.000 iteration steps during initialization and 30.000 iterations per annealing step.

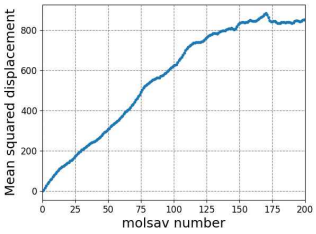

(i) 400.000 iteration steps during initialization and 40.000 iterations per annealing step.

Figure 3.15: Mean square displacement of the cobalt particle on a FCC(111) support with a weak metal-support interaction strength (D_e = 35 kcal/mol) and a different number of iterations during initialization and iteration steps.

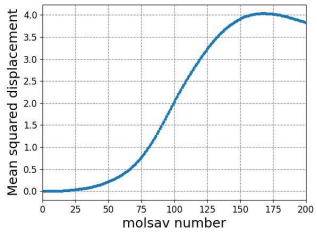

(a) 1.000 iteration steps during initialization and 100 iterations per annealing step.

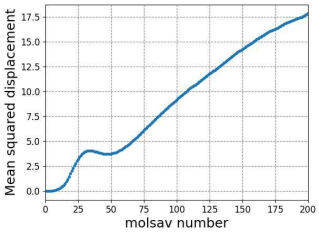

(b) 5.000 iteration steps during initialization and 500 iterations per annealing step.

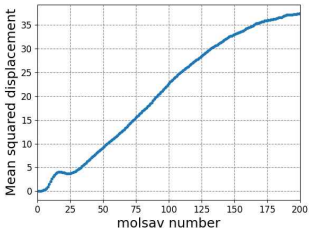

(c) 10.000 iteration steps during initialization and 1.000 iterations per annealing step.

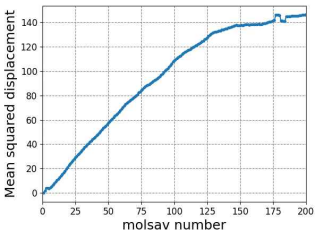

(d) 50.000 iteration steps during initialization and 5.000 iterations per annealing step.

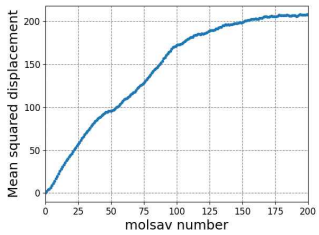

(e) 100.000 iteration steps during initialization and 10.000 iterations per annealing step.

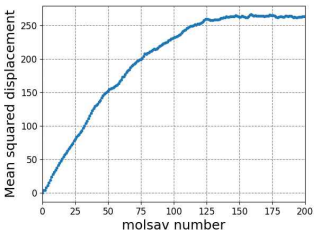

(f) 150.000 iteration steps during initialization and 15.000 iterations per annealing step.

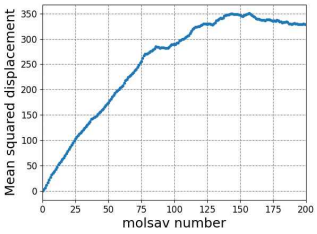

(g) 200.000 iteration steps during initialization and 20.000 iterations per annealing step.

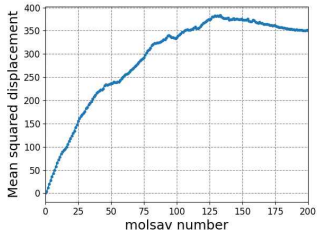

(h) 300.000 iteration steps during initialization and 30.000 iterations per annealing step.

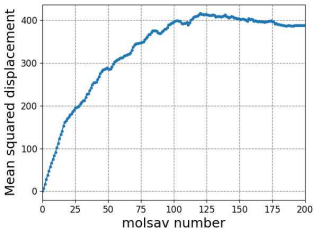

(i) 400.000 iteration steps during initialization and 40.000 iterations per annealing step.

Figure 3.16: Mean square displacement of the cobalt particle on a FCC(111) support with a moderate metal-support interaction strength (D_e = 40 kcal/mol) and a different number of iterations during initialization and iteration steps.

(a) 1.000 iteration steps during initialization and 100 iterations per annealing step.

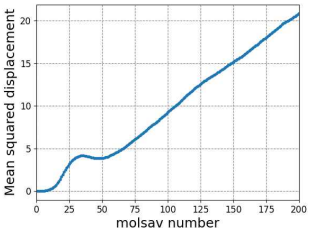

(b) 5.000 iteration steps during initialization and 500 iterations per annealing step.

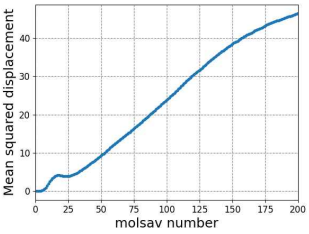

(c) 10.000 iteration steps during initialization and 1.000 iterations per annealing step.

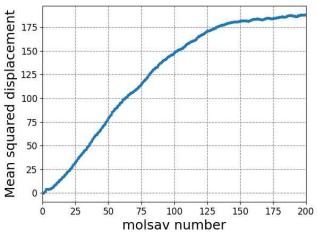

(d) 50.000 iteration steps during initialization and 5.000 iterations per annealing step.

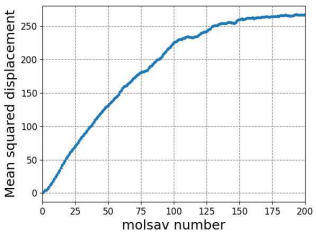

(e) 100.000 iteration steps during initialization and 10.000 iterations per annealing step.

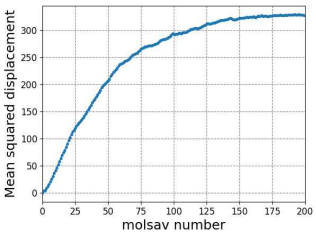

(f) 150.000 iteration steps during initialization and 15.000 iterations per annealing step.

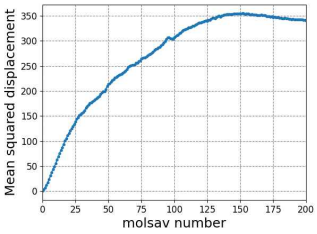

(g) 200.000 iteration steps during initialization and 20.000 iterations per annealing step.

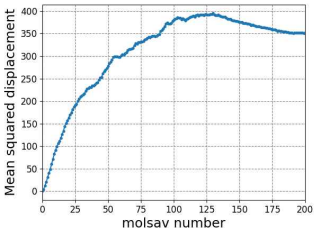

(h) 300.000 iteration steps during initialization and 30.000 iterations per annealing step.

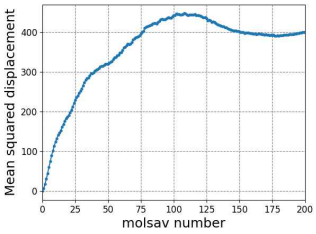

(i) 400.000 iteration steps during initialization and 40.000 iterations per annealing step.

Figure 3.17: Mean square displacement of the cobalt particle on a FCC(111) support with a moderate metal-support interaction strength (D_e = 45 kcal/mol) and a different number of iterations during initialization and iteration steps.

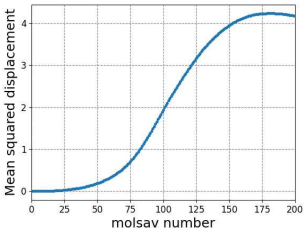

(a) 1.000 iteration steps during initialization and 100 iterations per annealing step.

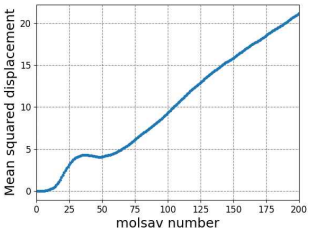

(b) 5.000 iteration steps during initialization and 500 iterations per annealing step.

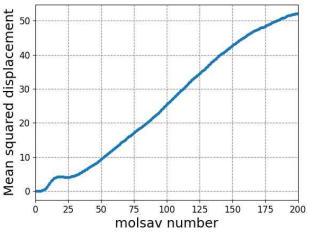

(c) 10.000 iteration steps during initialization and 1.000 iterations per annealing step.

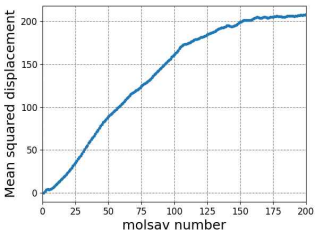

(d) 50.000 iteration steps during initialization and 5.000 iterations per annealing step.

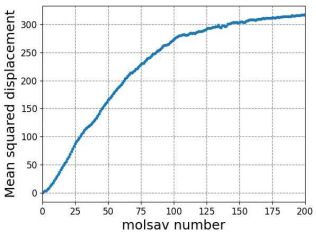

(e) 100.000 iteration steps during initialization and 10.000 iterations per annealing step.

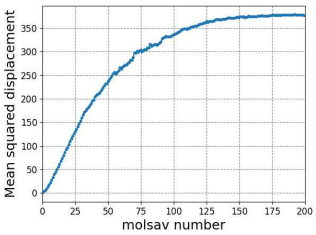

(f) 150.000 iteration steps during initialization and 15.000 iterations per annealing step.

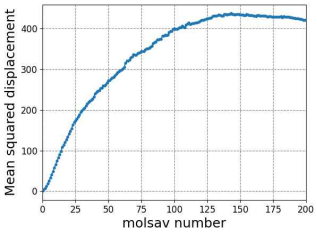

(g) 200.000 iteration steps during initialization and 20.000 iterations per annealing step.

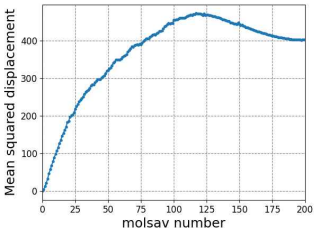

(h) 300.000 iteration steps during initialization and 30.000 iterations per annealing step.

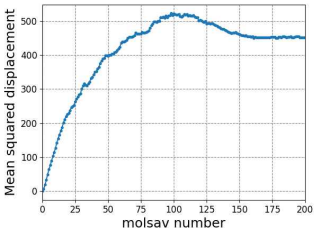

(i) 400.000 iteration steps during initialization and 40.000 iterations per annealing step.

Figure 3.18: Mean square displacement of the cobalt particle on a FCC(111) support with a strong metal-support interaction strength (D_e = 50 kcal/mol) and a different number of iterations during initialization and iteration steps.

3.4 Particle size

The number of atoms in the annealing simulations with a support are compatible with the number of atoms used in the annealing simulations without support in the work performed by van Etten et al. [11]. However, the size of the particles formed via the annealing simulations in presence of a support is not compatible with the particle size of the same number of atoms in the annealing simulations performed by van Etten et al. [11]. This is due to the different metal-support interactions. From Figure 3.19, it can be seen that when the metal-support interaction strength is weak, spherical like nanoparticles are formed. With an increasing metal support interaction strength the nanoparticles are forming a "pancake like" shape which increases the particle size. Therefore, the particle size has to be determined for the different number of atoms and the different metal-support interaction strengths.

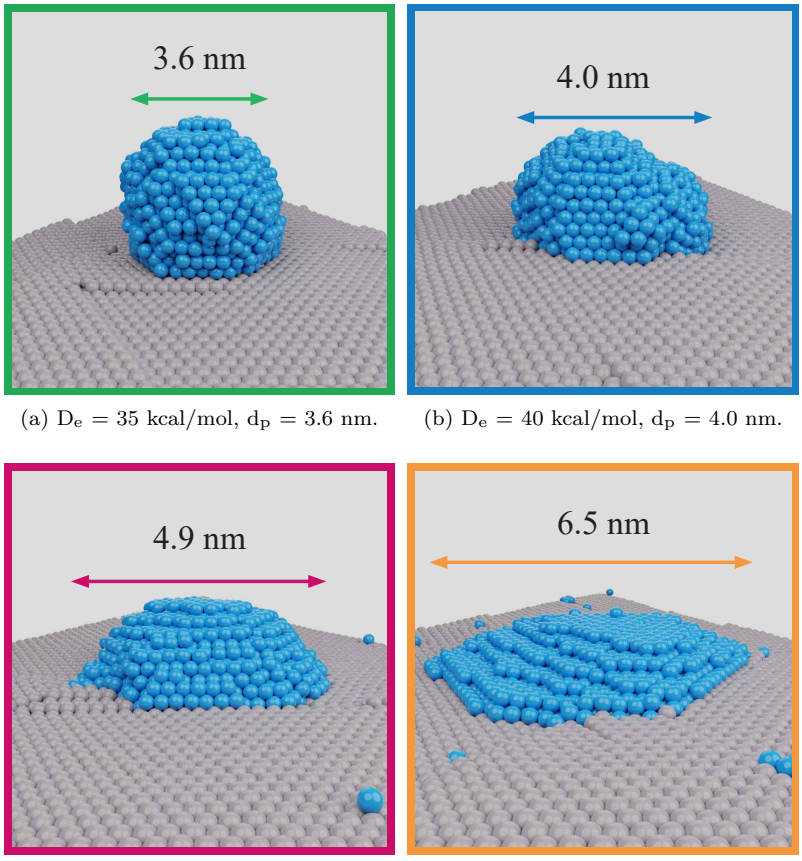

(a) D_e = 35 kcal/mol, d_p = 3.6 nm. (b) D_e = 40 kcal/mol, d_p = 4.0 nm.

(c) D_e = 45 kcal/mol, d_p = 4.9 nm. (d) D_e = 50 kcal/mol, d_p = 6.5 nm.

Figure 3.19: Cobalt particle of 12×12×12 atoms on an FCC(111) support with different interaction strengths.

To determine the particle size of the particle, the coordinates of the atoms on the edge of the particle have to be obtained. This is done by analysing the positions of the atoms after the annealing simulations. The size of the particle is then calculated via Equation 3.3. To obtain a more precise diameter, five samples per different particle size were used to determine the average particle sizes.

$$d_p = \sqrt{(x_1 - x_2)^2 + (y_1 - y_2)^2} \tag{3.3}$$

Table 3.2, presents the average diameter for the different number of atoms and metal-support interaction strengths compared to the results obtained by van Etten et al. [11]. In Appendix C, Table 3.2 can be found with the the corresponding errors corresponding to the 95% confidence interval. As can be seen from Table 3.2 the particle size of a weak metal-support interaction strength (D_e = 35 kcal/mol) is almost compatible with the particle size obtained by van Etten et al. [11]. This was expected, since the weak metal-support interaction allows the cobalt atoms to form an almost perfect spherical particle which is compatible to the spherical shape of the cobalt particles obtained by van Etten et al. [11]. However, for stronger metal-support interaction strengths it can be seen that the particle size increases significantly compared to the weak metal-support interaction. This is due to the "pancake-like" shape which is formed by strong metal-support interactions.

Table 3.2: Particle size of different number of atoms by different metal-support interactions and without support.

Number of cobalt atoms	d_p (nm) D_e = 35 (kcal/mol)	d_p (nm) D_e = 40 (kcal/mol)	d_p (nm) D_e = 45 (kcal/mol)	d_p (nm) D_e = 50 (kcal/mol)	d_p (nm) by van Etten et al. [11]
$5 \times 5 \times 5$	1.3	1.7	2.0	2.7	1.4
$6 \times 6 \times 6$	1.7	2.0	2.5	3.0	1.7
$7 \times 7 \times 7$	2.0	2.3	2.9	3.9	2.1
$8 \times 8 \times 8$	2.2	2.7	3.3	4.4	2.4
$9 \times 9 \times 9$	2.5	3.0	3.7	4.9	2.7
$10 \times 10 \times 10$	3.0	3.4	4.1	5.7	3.0
$11 \times 11 \times 11$	3.2	3.8	4.5	6.0	3.3
$12 \times 12 \times 12$	3.6	4.0	4.9	6.5	3.6
$14 \times 14 \times 14$	4.1	4.6	5.7	7.3	4.2
$16 \times 16 \times 16$	4.8	5.5	6.6	8.0	4.8
$18 \times 18 \times 18$	5.3	6.2	7.1	9.3	5.4

3.5 Dispersion

Since the Fischer-Tropsch synthesis takes place on the surface of the catalyst, it is of great value to have a high dispersion. The dispersion is the ratio between the surface atoms and the total amount of atoms and can be calculated via Equation 3.4. In Equation 3.4 N_s represent the number of metal atoms at the surface and N_v represents the number of metal atoms in the bulk [4].

$$D \equiv \frac{N_s}{N_v} \tag{3.4}$$

It is expected that the dispersion of the cobalt atoms increases with the increasing metal-support interaction strength. This is due to the 'pancake-like' shape which allows more cobalt atoms to be present at the surface instead of in the bulk. Figure 3.20 shows the dispersion as function of particle size for each of the simulated metal-support interaction strengths. The black dots indicate the dispersion values obtained by van Etten et al. [11] for unsupported nanoparticles. As can be seen from Figure 3.20 the dispersion increases when the metal-support interaction increases. It was expected that the weak metal-support interaction follows almost the same trend as the dispersion trend obtained for unsupported nanoparticles. However, it can be seen that the dispersion for the supported nanoparticles with weak metal-support interactions is slightly lower than that obtained for nanoparticles in vacuum. This is due to the presence of the support. Since the cobalt nanoparticle in vacuum does not have a support, it can hold more surface atoms than with a support. It can also be seen that the dispersion of the surface atoms is higher at low particle size than at high particle size. This is due to the ratio between the amount of cobalt atoms that are in contact with the support and the amount of cobalt atoms at the surface. The number of bulk atoms connected to the support increases much slower compared to the surface atoms of cobalt with increasing number of particles.

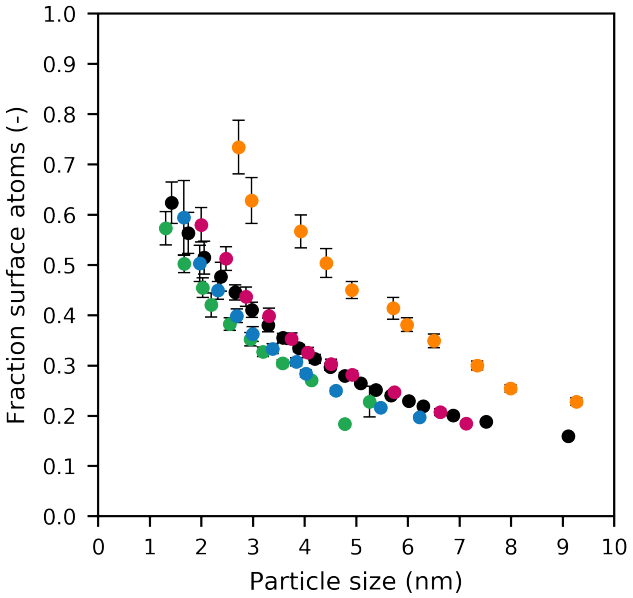

Figure 3.20: Fraction of the surface atoms (dispersion). Note that the green, blue, pink and orange represent the different metal-support interaction strengths from weak to strong respectively and the black dots correspond to the cobalt nanoparticles in vacuum. The error bars correspond to the 95% confidence interval.

3.6 Surface site distributions

In this section, the results of the annealing simulations will be analyzed. The different sites are identified using the pattern algorithm based on CNA [15] explained in Chapter 2.3. The average surface site distribution is obtained by averaging the site fractions of the 40 simulations per particle size over the whole particle size range. The error bars are corresponding to the 95% confidence interval. Research performed by van Etten et al. [11] has shown that for a nanoparticle in vacuum, the FCC(111) and FCC(100)-oriented terrace sites and the FCC(211) and FCC(110)-oriented step-edge sites show an increasing surface site fraction with increasing particle size up to ∼6 nm. After ∼6 nm a plateau is observed. This trend is similar to the structure sensitivity trend which is experimentally observed [8][9][10]. For the HCP(01-12) and HCP(03-31)-oriented step-edge sites the maximum surface site fraction is observed at a particle size of ∼3 nm. For the HCP(01-11)-oriented step-edge site a maximum surface site fraction is observed at a particle size of ∼2 nm. The HCP(01-13)-oriented step-edge sites are present in the whole range of particle sizes, however, the surface site fraction is very low.

3.6.1 FCC(110)-oriented step-edge sites

As can be seen from Figure 3.21, the trend of the surface site fraction follows the same trend as the experimentally obtained structure sensitivity trend. There is almost no difference between the different metal-support interaction strengths for the FCC(110)-oriented step-edge site.

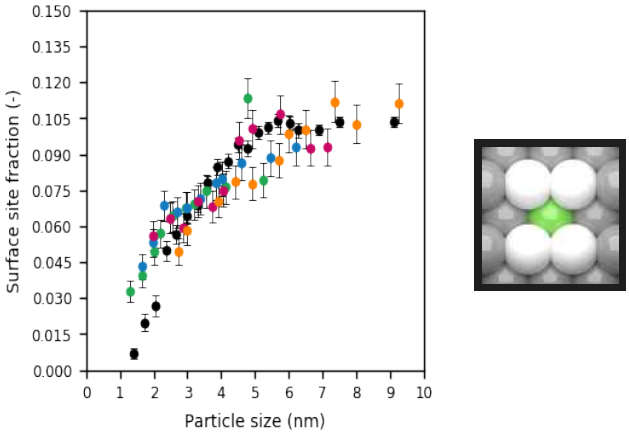

Figure 3.21: Surface site distribution of the FCC(110)-oriented step-edge sites. Note that the green, blue, pink and orange represent the different metal-support interaction strengths from weak to strong, respectively, and the black dots correspond to the cobalt nanoparticles in vacuum. The error bars correspond to the 95% confidence interval.

3.6.2 HCP(03-31)-oriented step-edge sites

As can be seen from Figure 3.22, the trend of the surface site fraction follows the same trend as the experimentally obtained structure sensitivity trend. However, the results show that the plateau starts at ∼3 nm instead of ∼6 nm which is experimentally obtained. It can be seen that for moderate interaction strengths the surface site fraction is higher than for weak and strong metal-support interaction strengths.

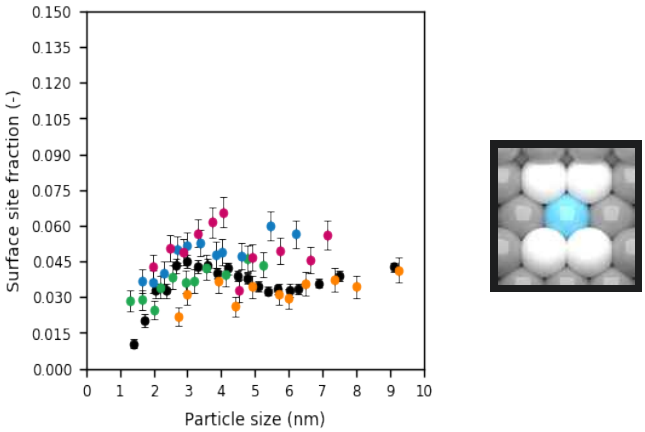

Figure 3.22: Surface site distribution of the HCP(03-31)-oriented step-edge sites. Note that the green, blue, pink and orange represent the different metal-support interaction strengths from weak to strong, respectively, and the black dots correspond to the cobalt nanoparticles in vacuum. The error bars correspond to the 95% confidence interval.

3.6.3 HCP(01-13)-oriented step-edge sites

As can be seen from Figure 3.23, the trend of the surface fraction follows the same trend as the obtained trend by van Etten et al. [11]. The HCP(01-13)-oriented step-edge sites are present with a low surface site fraction over the whole range of particle sizes. There is almost no difference between the different metal-support interaction strengths. However, for a weak metal-support interaction strength the surface site fraction of the HCP(01-13)-oriented step-edge sites is higher compared to the other metal-support interaction strengths and for a cobalt nanoparticle in vacuum.

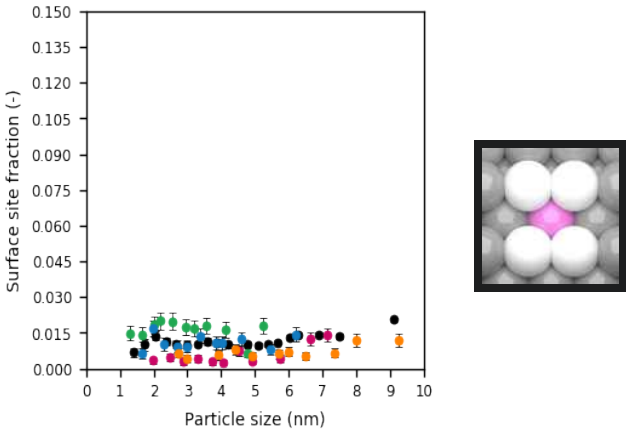

Figure 3.23: Surface site distribution of the HCP(01-13)-oriented step-edge sites. Note that the green, blue, pink and orange represent the different metal-support interaction strengths from weak to strong, respectively, and the black dots correspond to the cobalt nanoparticles in vacuum. The error bars correspond to the 95% confidence interval.

3.6.4 FCC(111)-oriented terrace sites

From Figure 3.24, it can be seen that a weak metal-support interaction strength has a low and constant surface fraction of the FCC(111)-oriented terrace sites, which is lower than the surface site fractions as obtained from cobalt nanoparticles in vacuum. The moderate metal-support interaction strengths have a higher surface fraction of the FCC(111)-oriented terrace sites for particle sizes below ∼4 nm. However, the surface site fraction for the FCC(111)-oriented terrace sites is decreasing onwards. The strong metal-support interaction strengths have a high surface site fraction for small particles and a low surface site fraction for large particles. The trend of the surface site fraction of the cobalt nanoparticle in vacuum is compared to the experimentally obtained structure sensitivity trend. However, this trend cannot be observed for each of the different metal-support interaction strengths.

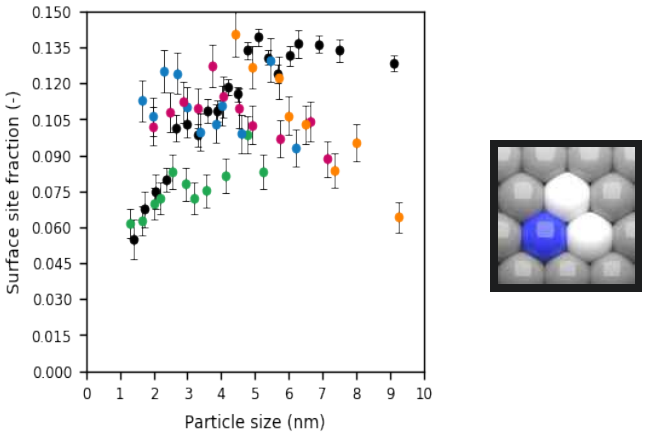

Figure 3.24: Surface site distribution of the FCC(111)-oriented terrace sites. Note that the green, blue, pink and orange represent the different metal-support interaction strengths from weak to strong, respectively, and the black dots correspond to the cobalt nanoparticles in vacuum. The error bars correspond to the 95% confidence interval.

3.6.5 FCC(100)-oriented terrace sites

As can be seen from Figure 3.25, the trend of the surface fractions follow the same trend as the experimentally obtained structure sensitivity trend. However, the plateau can be observed at ∼3 nm for weak metal-support interactions and a higher plateau at ∼2 nm for moderate metal-support interactions. For strong metal-support interactions the FCC(100)-oriented terrace sites have a low surface fraction which is slowly increasing with increasing particle size. Overall, the surface site fraction trend of all the different metal-support interaction strengths have a lower surface site fraction than obtained by a cobalt nanoparticle in vacuum.

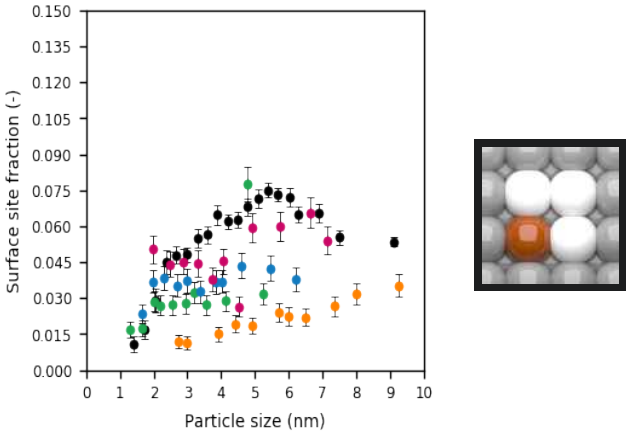

Figure 3.25: Surface site distribution of the FCC(100)-oriented terrace sites. Note that the green, blue, pink and orange represent the different metal-support interaction strengths from weak to strong, respectively, and the black dots correspond to the cobalt nanoparticles in vacuum. The error bars correspond to the 95% confidence interval.

3.6.6 FCC(211)-oriented step-edge sites

It can be seen from Figure 3.26, that weak metal-support interactions have a plateau over the whole particle size range for the FCC(221)-oriented step-edge sites. Strong metal-support interactions follow the trend of the experimentally obtained structure sensitivity trend and has a higher surface site fraction by larger particle sizes.

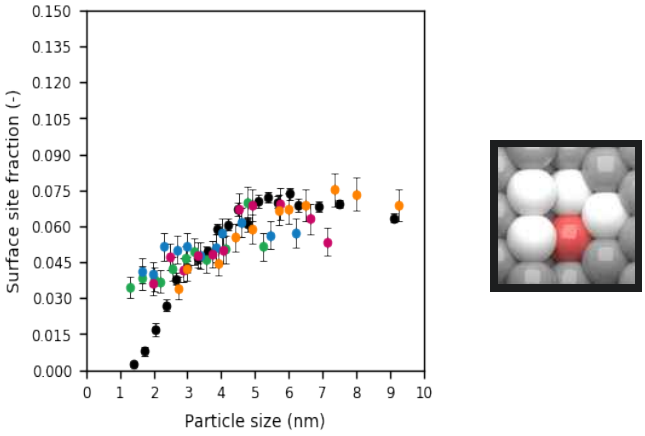

Figure 3.26: Surface site distribution of the FCC(211)-oriented step-edge sites. Note that the green, blue, pink and orange represent the different metal-support interaction strengths from weak to strong, respectively, and the black dots correspond to the cobalt nanoparticles in vacuum. The error bars correspond to the 95% confidence interval.

3.6.7 HCP(01-12)-oriented step-edge sites

As can be seen from Figure 3.27, the surface site fraction increases with increasing particle size up to ∼3 nm and shows a slightly decreasing plateau onwards. There is almost no difference between the different metal-support interactions. However, the surface site fractions obtained by the moderate metal-support interaction strengths is slightly higher compared to the weak and strong metal-support interaction strengths. Also it can be seen that the surface site fraction for the moderate metal-support interaction strengths is slightly higher compared to the surface site fraction obtained for the cobalt nanoparticle in vacuum.

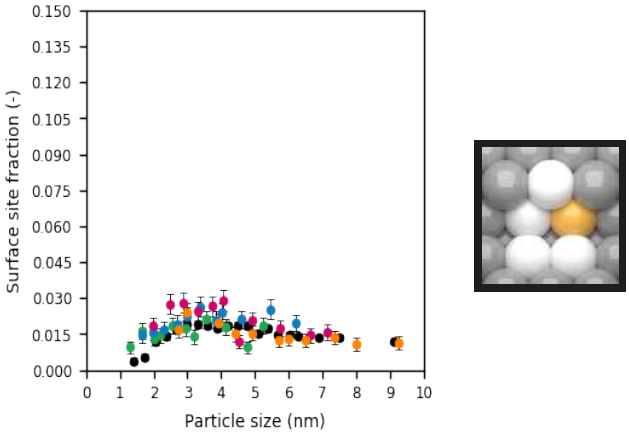

Figure 3.27: Surface site distribution of the HCP(01-12)-oriented step-edge sites. Note that the green, blue, pink and orange represent the different metal-support interaction strengths from weak to strong, respectively, and the black dots correspond to the cobalt nanoparticles in vacuum. The error bars correspond to the 95% confidence interval.

3.6.8 HCP(01-11)-oriented step-edge sites

As can be seen from Figure 3.28, the obtained results by van Etten et al. [11] show that there is an optimum at ∼2 nm. Subsequently, the surface fraction decreases. However, the weak metal-support interaction strength does not follow this trend. For a weak metal-support interaction strength the same trend as for the experimentally observed structure sensitivity trend is obtained. For stronger metal-support interaction strengths there is almost no difference in the surface site fraction over the whole range of particle sizes. However, a slight decrease of the surface site fraction can be observed after ∼ 5 nm for a strong metal-support interaction strength. Overall, the surface site fraction of the different metal-support interaction strengths is higher after ∼3 nm compared to the surface site fraction obtained by the cobalt nanoparticle in vacuum.

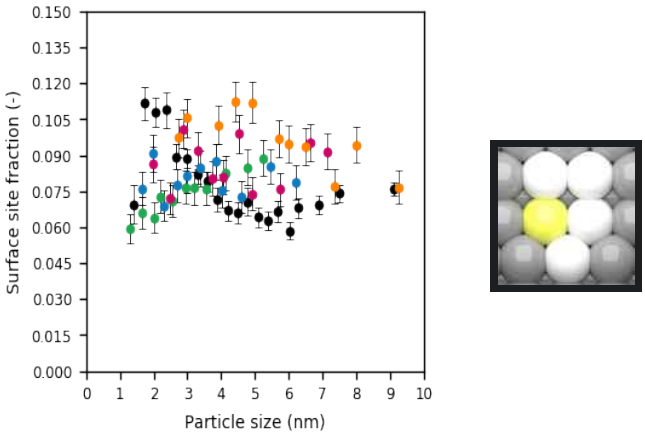

Figure 3.28: Surface site distribution of the HCP(01-11)-oriented step-edge sites. Note that the green, blue, pink and orange represent the different metal-support interaction strengths from weak to strong, respectively, and the black dots correspond to the cobalt nanoparticles in vacuum. The error bars correspond to the 95% confidence interval.

3.7 Turnover frequency

The activity of a specific site is of importance for comparing the catalysts with different metals, or as in this thesis with different metal-support interaction strength. For the comparison, the turnover frequency (TOF) is defined. The TOF is the number of reactant molecules converted over this site per second [4]. The turn over frequency per specific site is calculated via Equation 3.5. Within Equation 3.5, x_i represents the site fraction of the specific surface site i and r_i represents the corresponding site-based reaction rate.

$$TOF_i = x_i \cdot r_i \tag{3.5}$$

The total turn over frequency for the catalyst particle is calculated via Equation 3.6.

$$TOF_{total} = \sum_{i=1}^{n} TOF_i \tag{3.6}$$

The site-based reaction rates for the different surface sites are calculated by van Etten et al. [11] and can be found in Appendix D. Figure 3.29 presents the total activity for the different particle sizes and different metal-support interactions. As can be seen from Figure 3.29, all different metal-support interaction strengths follow the same trend. However, the trend for the total activity for the moderate metal-support interaction strengths lies slight higher than the total activity trends for the weak and strong metal-support interaction strengths. The trend which can be observed from Figure 3.29, also follows the same trend which is experimentally observed [8][9][10]. The total activity increases with increasing particle size up to ∼6 nm after which a plateau is observed. However, for a weak metal-support interaction the plateau is not visible since the lack of data points after ∼5 nm. This is due to the amount of atoms needed to produce a particle which is larger than ∼5 nm. The simulated annealing calculations would take too long to produce this results.

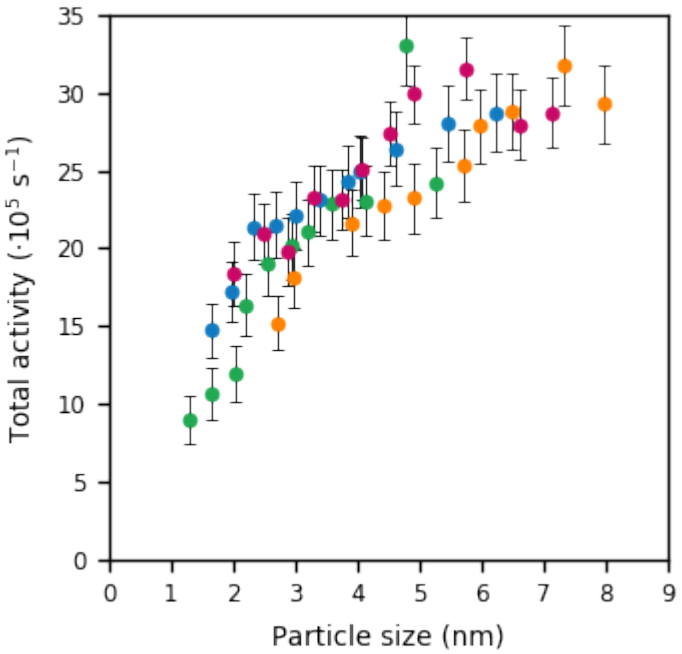

Figure 3.29: Total activity for different metal-support interaction strengths.

Figures 3.30 - 3.33, present the individual contributions from the different sites on the total activity of the particles with different metal-support interaction strengths. As can be seen from Figures 3.30 - 3.33, the contribution of the FCC(110)-oriented step-edge site is the highest, followed by the HCP(013)-oriented step-edge site. The contribution of the FCC(110)-oriented step-edge site is increasing with increasing particle size. However, the contribution of the HCP(013)-oriented step-edge site is decreasing with increasing particle size. From Figure 3.33, it can be seen that the contribution of the FCC(111)-oriented terrace site activity for a strong metal-support interaction strength is larger compared to the other metal-support interactions. This is due to the strong metal-support interaction strength on which the small number of atoms almost form a "pancake like" shape on the FCC(111)-oriented support. Therefore, there might be a little bias towards the FCC(111)-oriented terrace site with strong metal-support interactions if an FCC(111)-oriented structured support is used. However, the contribution of the FCC(111)-oriented terrace sites on the total activity is less than 10 % of the total activity, therefore, it is expected that there is no or little bias as a result of the FCC(111)-oriented terrace site. The error bars corresponding to the 95% confidence intervals were left out of Figure 3.30 - 3.33 to keep the Figures more clear. In Appendix E-H tables are presented with contribution of the different sites to the total TOF with different metal-support interaction strengths and the corresponding errors corresponding to the 95% confidence intervals. The overall observation is that the total activity for the different metal-support interaction strengths each follow the same trend as the experimentally observed structure sensitivity in cobalt based Fischer-Tropsch synthesis, and the majority of the activity is determined by the FCC(110)-oriented step-edge site. These findings suggest that the strength of the metal-support interaction does not have a significant influence on the obtained structure sensitivity trend.

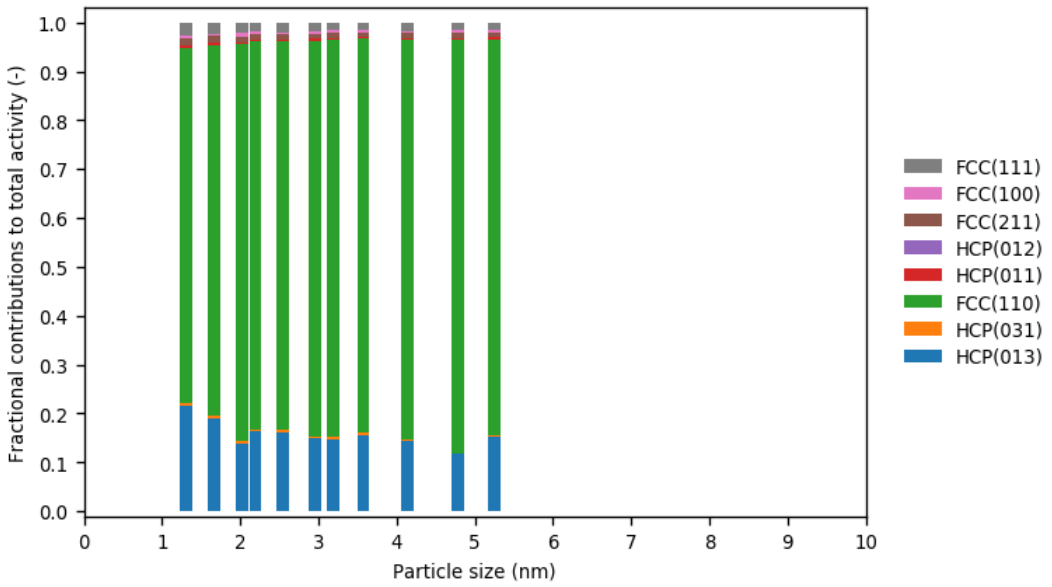

Figure 3.30: Contribution of the different sites to the total TOF for a weak metal-support interaction strength (D_e = 35 kcal/mol).

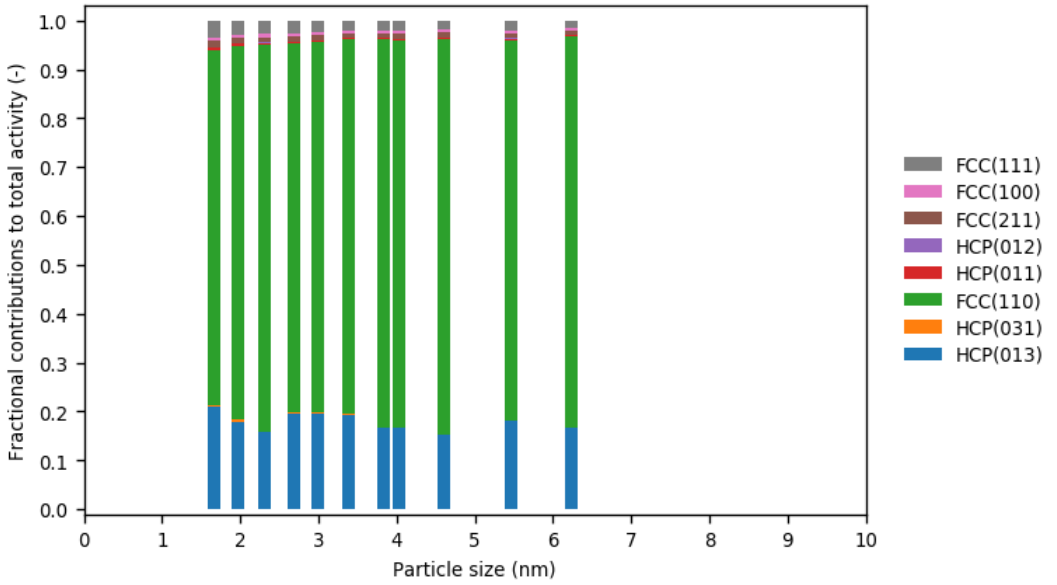

Figure 3.31: Contribution of the different sites to the total TOF for a moderate metal-support interaction strength (D_e = 40 kcal/mol).

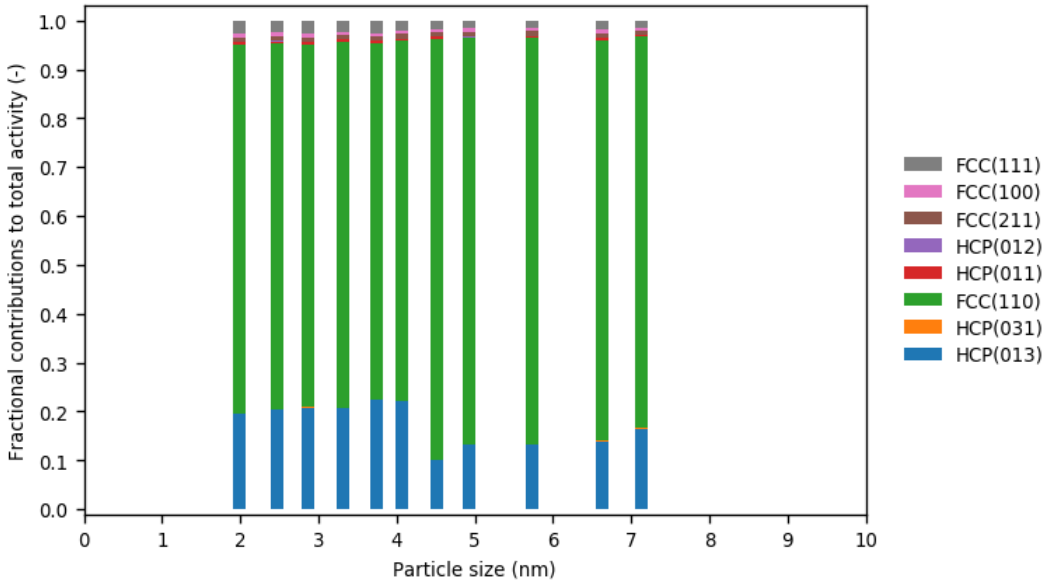

Figure 3.32: Contribution of the different sites to the total TOF for a moderate metal-support interaction strength (D_e = 45 kcal/mol).

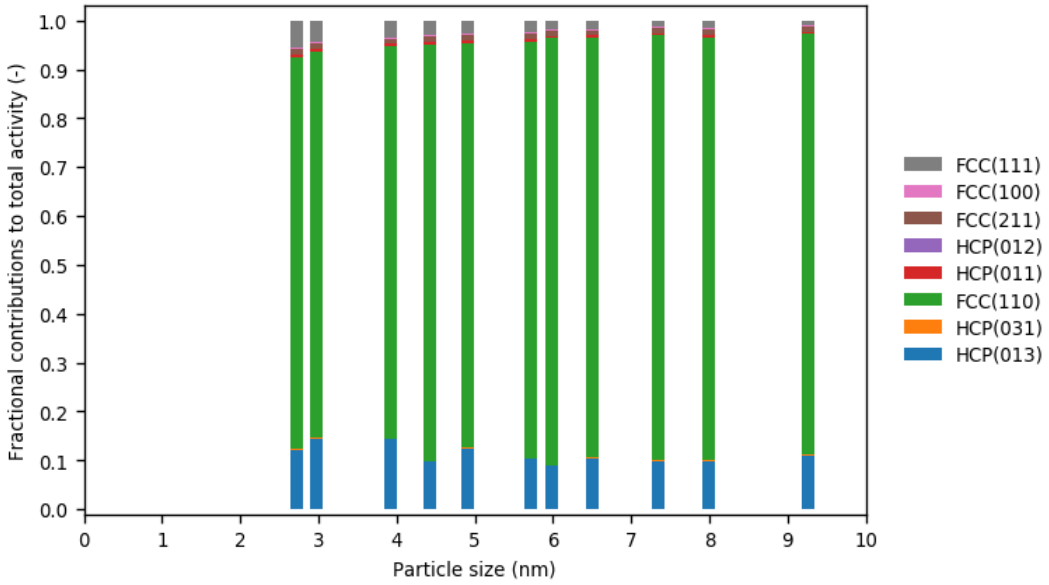

Figure 3.33: Contribution of the different sites to the total TOF for a strong metal-support interaction strength (D_e = 50 kcal/mol).

Chapter 4

Conclusion

The aim of this study was to understand the support effect on the structure sensitivity of cobalt-based Fischer-Tropsch synthesis. To understand the support effect on the structure sensitivity of cobalt-based Fischer-Tropsch synthesis, several methods have been used.
First, a ReaxFF force field is developed by extending an existing ReaxFF force field with a fictitious support material. The interaction strength could be tuned via changing a single parameter, namely, the dissociation energy (D_e). By changing the D_e in a range of 35 kcal/mol to 50 kcal/mol, the wetting effects due to metal-support interactions have been simulated, via simulated annealing calculations.
For the simulated annealing calculations, different settings have to be determined to suppress the computational time of the simulations. First, the size of the support was optimized on the basis of the strong metal-support interaction case. The support size of 4 times the number of atoms in the x- and y-direction of cobalt was chosen to be sufficient for the simulated annealing calculations. Secondly, the initial temperature of the simulated annealing simulations was altered. This was done to assure that the initialization period was performed at a sufficiently high temperature in order for the cobalt atoms to move out of their initial lattice. An initial temperature of 1500 K was sufficient for the simulated annealing simulations, since this would lead to the least amount of unknown sites recognized by the pattern recognition algorithm. Third, the number of iteration steps during initialization and the subsequent annealing trajectories were altered, to investigate if both the initialization and cooling trajectories were sufficiently long. This was done by investigating the number of unknown sites by the pattern recognition algorithm and via the mean square displacement of the atoms. Both methods concluded that 400.000 iterations during initialization and 40.000 iterations per annealing step of 100 K were sufficient.
The particle sizes of the nanoparticles formed via the simulated annealing calculations have been determined. It could be seen that the particle size increases with increasing metal-support interaction strength. This is due to shape of the nanoparticles. For a weak metal-support interaction strength spherical like nanoparticles were formed, whereas, for strong metal-support interaction strength "pancake like" nanoparticles were formed.
The dispersion for the different particle sizes and different metal-support interaction strengths have been investigated. It could be seen that the dispersion decreases with increasing particle size for each of the simulated metal-support interaction strengths. This is due to the faster increasing amount of bulk atoms compared to the surface atoms. It could also be seen that the dispersion increases with increasing metal-support interaction strength at a constant particle size. This is due to the shape of the nanoparticles which are formed. With a strong-metal support interaction strength, the nanoparticles will have a "pancake like" shape which contains more surface atoms than a spherical like nanoparticle, which is formed with a weak metal-support interaction strength.
The surface site distribution for the different sites has been analysed for different metal-support interaction strengths and was compared to the obtained surface site distribution for cobalt nanoparticle in vacuum. It has been shown that the FCC(211) and FCC(110)-oriented step-edge sites show an increasing surface site fraction with increasing particle size up to $\sim$6 nm, and a plateau is

observed onwards. This trend is similar to the structure sensitivity trend which is experimentally observed. For the HCP(01-12) and HCP(03-31)-oriented step-edge sites the maximum surface site fraction is observed at a particle size of ∼3 nm. For the HCP(01-11)-oriented step-edge site a maximum surface site fraction is observed at a particle size of ∼2 nm for the cobalt nanoparticle in vacuum. For a weak metal-support interaction strength the surface site fraction increases with increasing particle size. For moderate and strong metal-support interactions the surface site fraction does not changes with increasing particle size. The HCP(01-13)-oriented step-edge sites are present in the whole range of particle sizes, however, the surface site fraction is very low. This trend can be observed for all different metal-support interaction strengths as well as the cobalt nanoparticle in vacuum. It has been shown that for the FCC(111)-oriented terrace sites the surface fraction increases with increasing particle size for a cobalt particle in vacuum. However, a different trend was observed for the different metal-support interaction strengths. For a weak metal-support interaction a low and constant surface fraction could be observed. For moderate metal-support interactions a higher, slightly decreasing surface fraction could be observed. For a strong metal-support interaction strength a high surface fraction could be observed for small particle sizes and a lower surface fraction for smaller particle sizes. It has been shown that for the FCC(100)-oriented terrace sites the surface fraction increases with increasing particle size for a cobalt particle in vacuum and for the different metal-support interaction strengths. However, for weak metal-support interaction strengths the plateau is observed at ∼3 nm and for moderate metal-support interaction strengths at ∼2 nm. The surface fraction of the FCC(100)-oriented terrace sites for moderate metal-support interaction strengths is higher than for weak and strong metal-support interaction strengths.
Finally, the total activity of differently sized cobalt nanoparticles was calculated for the different metal-support interaction strengths. It could be seen that the total activity trend is the same for all different metal-support interaction strengths. However, the total activity for particles with a moderate metal-support interaction strength is slightly higher than for weak and strong metal-support interaction strengths.
In order to identify which site could be responsible for the overall activity in cobalt-based Fischer-Tropsch synthesis, the contribution of each of the identified surface sites to the overall activity was determined. The contributions of the FCC(110)-oriented step-edge site was significantly higher than all other contributions over the whole simulated metal-support interaction strength range. Therefore, it is expected that the FCC(110)-oriented step-edge sites are most likely responsible for the observed structure sensitivity trends in cobalt-based Fischer-Tropsch synthesis.

Chapter 5

Outlook

Extending an existing ReaxFF force field with a fictitious support material was a profound method to study the influence of the metal-support interaction strength on the structure sensitivity trend, however, some improvements can be made. First of all, a fictitious support has been used, due to the complexity it takes to create a force field for a specific support material and its interactions with cobalt. However, if such a force field was created, the metal-support interactions is determined by the interaction parameters in the force field. Therefore, multiple force fields have to be constructed in order to study the effect of metal-support interactions on structure sensitivity in cobalt-based Fischer-Tropsch synthesis.
Another improvement can be made by the orientation of the support. In this thesis an FCC(111)-oriented terrace site support was used to created less bias towards a specific surface site. However, to mimic a real, support surface roughness have to be added to the support layers. Since roughness of the support can influence the location and geometry of the formed cobalt nanoparticles.
The particle sizes were determined manually by measuring the particle size. For each of the simulated annealing simulations with a different number of atoms and a different metal-support interaction strength the particle size was determined by averaging over 5 particle sizes. Therefore, the determination of the particle size could have been more accurate. To improve the accuracy of the particle size more samples have to be taken to measure the particle size. Also, a script can be made to calculate the particle size for each simulation. However, there are some difficulties to take into account. For example, for strong metal-support interactions, some single cobalt atoms were observed on the support. Since these atoms are not part of the main particle, an overestimation of the particle size will be obtained when the particle size is determined by for example the maximum distance between two cobalt atoms.
For each of the metal-support interactions strengths, the same range in terms of cobalt atoms is simulated. However, the particle size range for weak metal-support interactions (1.5-5.5 nm) is significantly lower than that for strong metal-support interactions (2-9 nm). In order to obtain more insight in the structure sensitivity trends, a particle size range of around 2-9 nm is preferred, since both the experimentally observed increasing trend with increasing particle size up to around 6 nm as well as the plateau formation onwards can be observed. However, larger particle sizes for weak metal-support interaction strengths require a large number of atoms for the simulated annealing calculations. Since this would have resulted in too high computational costs, these simulations were not performed yet.

Acknowledgements

With my master thesis coming to an end, it is time to look back at the nine months I have been working on this project. I would like to take this opportunity to thank the people who helped me with my master thesis and made this year amazing. First of all, I would like to thank Emiel Hensen and Ivo Filot for giving me the opportunity to do my master thesis within the IMC group. I have learned a lot during these nine months. I even got to join the NCCC conference in March were I was selected to give a poster presentation, which was a great opportunity to learn how to present a poster. I would also like to thank Antoni Forner Cuenca for taking the time and effort to join the graduation committee of my master thesis.

Michel, I would like to thank you for your guidance during my master project. It was always nice to have both professional conversations about the project as well as the drinks after work hours. Not only is our name almost similar, we both have a similar preference on how a typical Thursday should look like. Of course, starting with a Triple Karmeliet in the F.O.R.T.

I would also like to thank the students in my office, Anouk, Jasper, Joost, Koen, Roos, Tim and Tom for spending the most time with me in the office and making these nine months more fun. I would like to thank Koen personally, since he helped me a lot during my project, even when we had to work from home due to the corona virus. The 3D models you made of my cobalt nanoparticles are really nice and have a prominent spot under the television.

Lastly, I would like to thank my parents and Alwin for always supporting me during my study and keeping me motivated.

Bibliography

[1] "Fossil Fuels - Our World in Data." [Online]. Available: https://ourworldindata.org/fossil-fuels#all-charts-preview 1

[2] "Transportation and Energy | The Geography of Transport Systems." [Online]. Available: https://transportgeography.org/?page_id=15592 1

[3] "Global energy demand will keep world burning fossil fuels, agency says." [Online]. Available: https://www.cnbc.com/2019/11/12/global-energy-demand-will-keep-world-burning-fossil-fuels-agency-says.html 1

[4] "Concepts of Modern Catalysis and Kinetics - Concepts of Modern Catalysis and Kinetics - Wiley Online Library." [Online]. Available: https://onlinelibrary.wiley.com/doi/pdf/10.1002/3527602658 2, 3, 32, 41

[5] R. Whyman, "Piet W. N. M. Van Leeuwen. Homogeneous catalysis—understanding the art. Kluwer, Dordrecht, 2004, 407 pp; (UK). ISBN 1-4020-1999-8," *Applied Organometallic Chemistry*, vol. 19, no. 8, pp. 994–994, 8 2005. [Online]. Available: http://doi.wiley.com/10.1002/aoc.939 2

[6] I. Filot, "Quantum chemical and microkinetic modeling of the Fischer-Tropsch reaction," Tech. Rep., 2015. [Online]. Available: www.tue.nl/taverne 3

[7] M. E. Dry, "The Fischer-Tropsch process: 1950-2000," in *Catalysis Today*, vol. 71, no. 3-4. Elsevier, 1 2002, pp. 227–241. 3

[8] G. L. Bezemer, J. H. Bitter, H. P. Kuipers, H. Oosterbeek, J. E. Holewijn, X. Xu, F. Kapteijn, A. J. Van Diilen, and K. P. De Jong, "Cobalt particle size effects in the Fischer-Tropsch reaction studied with carbon nanofiber supported catalysts," *Journal of the American Chemical Society*, vol. 128, no. 12, pp. 3956–3964, 3 2006. 4, 33, 41

[9] J. X. Liu, P. Wang, W. Xu, and E. J. Hensen, "Particle Size and Crystal Phase Effects in Fischer-Tropsch Catalysts," *Engineering*, vol. 3, no. 4, pp. 467–476, 8 2017. 4, 33, 41

[10] J. P. Den Breejen, P. B. Radstake, G. L. Bezemer, J. H. Bitter, V. Frøseth, A. Holmen, and K. P. De Jong, "On the origin of the cobalt particle size effects in Fischer-Tropsch catalysis," *Journal of the American Chemical Society*, vol. 131, no. 20, pp. 7197–7203, 5 2009. 4, 33, 41

[11] M. van Etten, B. Zijlstra, E. Hensen, and I. Filot, "Understanding particle size dependence of cobalt nanoparticle catalyzed CO bond activation." 4, 30, 31, 32, 33, 35, 40, 41, 55, 56

[12] C. H. Mejía, T. W. Van Deelen, and K. P. De Jong, "Activity enhancement of cobalt catalysts by tuning metal-support interactions." [Online]. Available: www.nature.com/naturecommunications 4

[13] A. Tavasoli, K. Sadagiani, F. Khorashe, A. A. Seifkordi, A. A. Rohani, and A. Nakhaeipour, "Cobalt supported on carbon nanotubes - A promising novel Fischer-Tropsch synthesis catalyst," *Fuel Processing Technology*, vol. 89, no. 5, pp. 491–498, 5 2008. 4

[14] T. W. Van Deelen, H. Su, N. A. J. M. Sommerdijk, K. P. De Jong, R. Li, and . Chemcomm, "Open Access Article," *2530 | Chem. Commun*, vol. 54, p. 2530, 2018. 4

[15] W. F. Reinhart, A. W. Long, M. P. Howard, A. L. Ferguson, and A. Z. Panagiotopoulos, "Machine learning for autonomous crystal structure identification," *Soft Matter*, vol. 13, p. 4733, 2017. 5, 8, 33

[16] A. C. T. Van Duin, S. Dasgupta, F. Lorant, and W. A. G. Iii, "ReaxFF: A Reactive Force Field for Hydrocarbons," 2001. [Online]. Available: https://pubs.acs.org/sharingguidelines 6, 7

[17] X.-Q. Zhang, E. Iype, S. V. Nedea, A. P. J. Jansen, B. M. Szyja, Emiel, J. M. Hensen, and R. A. Van Santen, "Site Stability on Cobalt Nanoparticles: A Molecular Dynamics ReaxFF Reactive Force Field Study," 1157. [Online]. Available: https://pubs.acs.org/sharingguidelines 6, 11

[18] K. D. Nielson, A. C. T. Van Duin, J. Oxgaard, W.-Q. Deng, and W. A. G. Iii, "Development of the ReaxFF Reactive Force Field for Describing Transition Metal Catalyzed Reactions, with Application to the Initial Stages of the Catalytic Formation of Carbon Nanotubes," 2005. [Online]. Available: https://pubs.acs.org/sharingguidelines 6, 25

[19] D. Alloyeau, C. Mottet, and C. Ricolleau, *Nanoalloys - Synthesis, Structure and Properties*, 2012. [Online]. Available: https://drive.google.com/open?id=1cWFOSk8yBesz1fmfdcTU8qJlNkO2VD9- 7

[20] D. J. Wales and H. A. Scheraga, "Global Optimization of Clusters, Crystals, and Biomolecules," Tech. Rep. [Online]. Available: http://science.sciencemag.org/ 7

[21] "Mersenne Twister - an overview | ScienceDirect Topics." [Online]. Available: https://www.sciencedirect.com/topics/computer-science/mersenne-twister 10

Appendix A

ReaxFF parameter overview

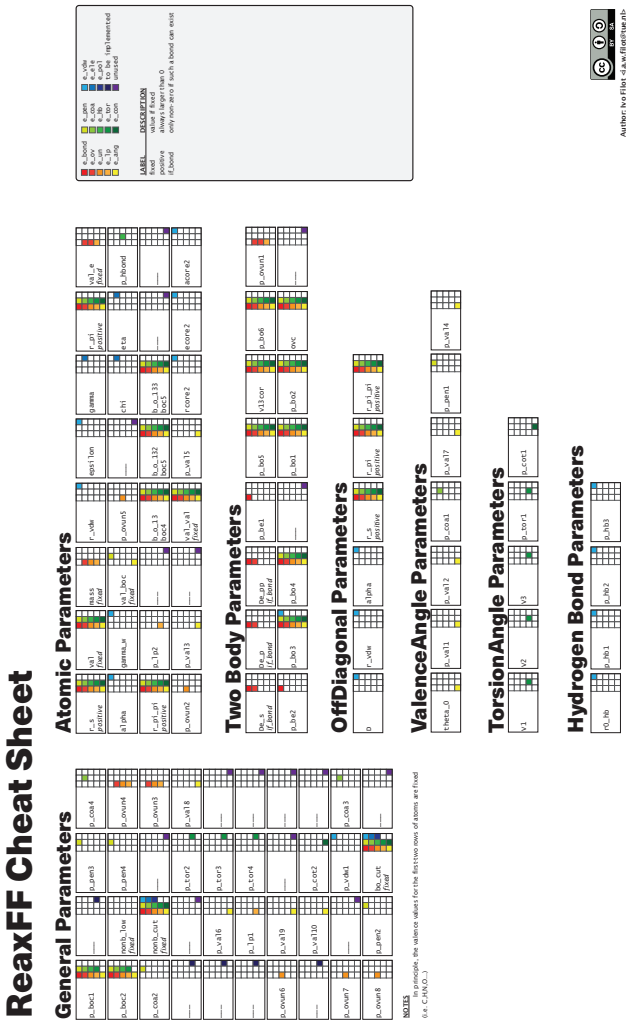

Appendix B

Parameters of the metal-support force field

```
Reactive MD-force field: Al force field/H2O force field
 39      ! Number of general parameters
  50.0000 !p(boc1)
   9.5469 !p(boc2)
  26.5405 !p(coa2)
   1.7224 !p(trip4)
   6.8702 !p(trip3)
   60.485 !kc2
   1.0588 !p(ovun6)
   4.6000 !p(trip2)
  12.1176 !p(ovun7)
  13.3056 !p(ovun8)
 -70.5044 !p(trip1)
   0.0000 !Lower Taper-radius (swa)
  10.0000 !Upper Taper-radius (swb)
   2.8793 !not used
  33.8667 !p(val7)
   6.0891 !p(lp1)
   1.0563 !p(val9)
   2.0384 !p(val10)
   6.1431 !not used
```

```
   6.9290 !p(pen2)
   0.3989 !p(pen3)
   3.9954 !p(pen4)
  -2.4837 !not used
   5.7796 !p(tor2)
  10.0000 !p(tor3)
   1.9487 !p(tor4)
  -1.2327 !not used
   2.1645 !p(cot2)
   1.5591 !p(vdW1)
   0.1000 !Cutoff for bond order*100 (cutoff)
   2.1365 !p(coa4)
   0.6991 !p(ovun4)
  50.0000 !p(ovun3)
   1.8512 !p(val8)
   0.5000 !not used
  20.0000 !not used
   5.0000 !not used
   0.0000 !not used
   2.6962 !p(coa3)
 3    ! Nr of atoms; cov.r; valency;a.m;Rvdw;Evdw;gammaEEM;cov.r2;#
        alfa;gammavdW;valency;Eunder;Eover;chiEEM;etaEEM;n.u.
        cov r3;Elp;Heat inc.;n.u.;n.u.;n.u.;n.u.
        ov/un;val1;n.u.;val3,vval4
 H    0.8930   1.0000   1.0080   1.3550   0.0930   0.8203  -0.1000   1.0000
      8.2230  33.2894   1.0000   0.0000 121.1250   3.7248   9.6093   1.0000
     -0.1000   0.0000  61.6606   3.0408   2.4197   0.0003   1.0698   0.0000
    -19.4571   4.2733   1.0338   1.0000   2.8793   0.0000   0.0000   0.0000
 Ni   2.4960   3.00009958.9330   1.7231   0.2328   0.8139   0.2089   3.0000
     12.6998  15.0031   3.0000   0.0000   0.0000   4.8038   7.3852   0.0000
     -0.9623   0.0000  96.9473   1.6928   4.3501   0.4034   0.8563   0.0000
     -2.5000   2.9330   1.0338   2.8790   2.5791   0.0000   0.0000   0.0000
```

```
Co   2.4960   3.0000  58.9330   1.7231   0.2328   0.8139   0.2089   3.0000
    12.6998  15.0031   3.0000   0.0000   0.0000   4.8038   7.3852   0.0000
    -0.9623   0.0000  96.9473   1.6928   4.3501   0.4034   0.8563   0.0000
    -2.5000   2.9330   1.0338   2.8790   2.5791   0.0000   0.0000   0.0000
 6     ! Nr of bonds; Edis1;LPpen;n.u.;pbe1;pbo5;13corr;pbo6
                  pbe2;pbo3;pbo4;n.u.;pbo1;pbo2;ovcorr
 1  1 153.3934   0.0000   0.0000  -0.4600   0.0000   1.0000   6.0000   0.7300
      6.2500   1.0000   0.0000   1.0000  -0.0790   6.0552   0.0000   0.0000
 1  2 160.0000   0.0000   0.0000  -0.5725   0.0000   1.0000   6.0000   0.5626
      1.1150   1.0000   0.0000   0.0000  -0.0920   4.2790   0.0000   0.0000
 2  2  53.5381   0.0000   0.0000  -0.2729  -0.2000   0.0000  16.0000   0.2915
      7.2786  -0.2000  15.0000   1.0000  -0.0976   7.9115   0.0000   0.0000
 1  3 107.4452   0.0000   0.0000  -0.6698  -0.3000   0.0000  36.0000   0.1543
      9.6122  -0.3500  25.0000   1.0000  -0.0867   7.1984   0.0000   0.0000
 2  3  35.0000   0.0000   0.0000  -0.2729  -0.2000   0.0000  16.0000   0.2915
      7.2786  -0.2000  15.0000   1.0000  -0.0976   7.9115   0.0000   0.0000
 3  3  53.5381   0.0000   0.0000  -0.2729  -0.2000   0.0000  16.0000   0.2915
      7.2786  -0.2000  15.0000   1.0000  -0.0976   7.9115   0.0000   0.0000
 0    ! Nr of off-diagonal terms; Ediss;Ro;gamma;rsigma;rpi;rpi2
 0    ! Nr of angles;at1;at2;at3;Thetao,o;ka;kb;pv1;pv2
 0    ! Nr of torsions;at1;at2;at3;at4;;V1;V2;V3;V2(BO);vconj;n.u;n
 0    ! Nr of hydrogen bonds;at1;at2;at3;Rhb;Dehb;vhb1
```

Appendix C

Particle size of different number of atoms by different metal-support interactions and without support

Number of cobalt atoms	d_p (nm) $D_e = 35$ (kcal/mol)	d_p (nm) $D_e = 40$ (kcal/mol)	d_p (nm) $D_e = 45$ (kcal/mol)	d_p (nm) $D_e = 50$ (kcal/mol)	d_p (nm) by van Etten et al. [11]
$5 \times 5 \times 5$	1.3 ± 0.23	1.7 ± 0.26	2.0 ± 0.28	2.7 ± 0.33	1.4
$6 \times 6 \times 6$	1.7 ± 0.26	2.0 ± 0.28	2.5 ± 0.32	3.0 ± 0.34	1.7
$7 \times 7 \times 7$	2.0 ± 0.28	2.3 ± 0.30	2.9 ± 0.34	3.9 ± 0.40	2.1
$8 \times 8 \times 8$	2.2 ± 0.30	2.7 ± 0.33	3.3 ± 0.36	4.4 ± 0.42	2.4
$9 \times 9 \times 9$	2.5 ± 0.32	3.0 ± 0.35	3.7 ± 0.39	4.9 ± 0.44	2.7
$10 \times 10 \times 10$	3.0 ± 0.34	3.4 ± 0.37	4.1 ± 0.40	5.7 ± 0.47	3.0
$11 \times 11 \times 11$	3.2 ± 0.36	3.8 ± 0.39	4.5 ± 0.42	6.0 ± 0.49	3.3
$12 \times 12 \times 12$	3.6 ± 0.38	4.0 ± 0.40	4.9 ± 0.44	6.5 ± 0.51	3.6
$14 \times 14 \times 14$	4.1 ± 0.41	4.6 ± 0.43	5.7 ± 0.48	7.3 ± 0.54	4.2
$16 \times 16 \times 16$	4.8 ± 0.44	5.5 ± 0.47	6.6 ± 0.51	8.0 ± 0.57	4.8
$18 \times 18 \times 18$	5.3 ± 0.46	6.2 ± 0.50	7.1 ± 0.53	9.3 ± 0.61	5.4

Appendix D

Site-specific activity and surface coverage of carbon monoxide, hydrogen, atomic carbon and empty sites

Site	TOF ($\times 10^5$ s^{-1})	Surface coverage (-) [11]			
		CO	H	C	*
FCC(111)	4.74	0.474	0.178	0.000	0.348
FCC(100)	3.47	0.005	0.066	0.582	0.347
FCC(211)	4.58	0.446	0.176	0.030	0.348
HCP(012)	0.39	0.000	0.020	0.661	0.319
HCP(011)	1.05	0.000	0.014	0.677	0.309
FCC(110)	246.82	0.473	0.178	0.000	0.348
HCP(031)	4.74	0.474	0.178	0.000	0.348
HCP(013)	84.42	0.473	0.178	0.000	0.348

Appendix E

Site contribution to total TOF (D_e = 35 kcal/mol)

	$5 \times 5 \times 5$	$6 \times 6 \times 6$	$7 \times 7 \times 7$	$8 \times 8 \times 8$
HCP(013)	0.215235 ± 0.031834	0.189679 ± 0.027918	0.138896 ± 0.022069	0.162961 ± 0.022015
HCP(031)	0.0063345 ± 0.001294	0.0053295 ± 0.001109	0.0057715 ± 0.001066	0.0053619 ± 0.000946
FCC(110)	0.7270412 ± 0.100041	0.7575203 ± 0.095396	0.8102500 ± 0.091141	0.7930165 ± 0.083038
HCP(011)	0.0055722 ± 0.000571	0.0054046 ± 0.000526	0.0044623 ± 0.000441	0.0043139 ± 0.000399
HCP(012)	0.0003347 ± 0.000085	0.0004964 ± 0.000097	0.0003413 ± 0.000074	0.0003178 ± 0.000066
FCC(211)	0.0141426 ± 0.001901	0.0136828 ± 0.001746	0.0115521 ± 0.001482	0.0095450 ± 0.001241
FCC(100)	0.0052721 ± 0.001010	0.0047047 ± 0.000891	0.0066202 ± 0.000977	0.0052615 ± 0.000802
FCC(111)	0.0260678 ± 0.002625	0.0231827 ± 0.002313	0.0221068 ± 0.002086	0.0192223 ± 0.001792

	$9 \times 9 \times 9$	$10 \times 10 \times 10$	$11 \times 11 \times 11$	$12 \times 12 \times 12$
HCP(013)	0.162407 ± 0.020741	0.149338 ± 0.019558	0.147977 ± 0.019277	0.156886 ± 0.019039
HCP(031)	0.0047350 ± 0.000839	0.0040539 ± 0.000764	0.0038681 ± 0.000739	0.0037598 ± 0.000698
FCC(110)	0.7944854 ± 0.078441	0.8093655 ± 0.077854	0.8116907 ± 0.077197	0.8064469 ± 0.073810
HCP(011)	0.0037491 ± 0.000351	0.0039028 ± 0.000353	0.0038194 ± 0.000345	0.0035038 ± 0.000317
HCP(012)	0.0003618 ± 0.000067	0.0003332 ± 0.000063	0.0002594 ± 0.000055	0.0003632 ± 0.000062
FCC(211)	0.0097350 ± 0.001183	0.0103479 ± 0.001199	0.0107388 ± 0.001210	0.0092605 ± 0.001077
FCC(100)	0.0047458 ± 0.000719	0.0047008 ± 0.000704	0.0053585 ± 0.000744	0.0041381 ± 0.000627
FCC(111)	0.0197810 ± 0.001715	0.0179579 ± 0.001607	0.0162880 ± 0.001515	0.0156414 ± 0.001425

	$14 \times 14 \times 14$	$16 \times 16 \times 16$	$18 \times 18 \times 18$
HCP(013)	0.144007 ± 0.018154	0.117981 ± 0.013712	0.151809 ± 0.018191
HCP(031)	0.0033582 ± 0.000657	0.0009439 ± 0.000291	0.0034845 ± 0.000653
FCC(110)	0.8174935 ± 0.073958	0.8463167 ± 0.062795	0.8099721 ± 0.071849
HCP(011)	0.0037577 ± 0.000327	0.0026972 ± 0.000231	0.0038565 ± 0.000323
HCP(012)	0.0003027 ± 0.000057	0.0001142 ± 0.000029	0.0003004 ± 0.000055
FCC(211)	0.0099990 ± 0.001114	0.0096834 ± 0.000915	0.0097535 ± 0.001074
FCC(100)	0.0043424 ± 0.000639	0.0081415 ± 0.000730	0.0045496 ± 0.000638
FCC(111)	0.0167393 ± 0.001467	0.0141221 ± 0.001124	0.0162741 ± 0.001411

Appendix F

Site contribution to the total TOF (D_e = 40 kcal/mol)

	$5 \times 5 \times 5$	$6 \times 6 \times 6$	$7 \times 7 \times 7$	$8 \times 8 \times 8$
HCP(013)	0.210976 ± 0.027506	0.178218 ± 0.023374	0.157452 ± 0.019717	0.195531 ± 0.021898
HCP(031)	0.0020811 ± 0.000647	0.0047142 ± 0.000901	0.0022751 ± 0.000562	0.0020472 ± 0.000531
FCC(110)	0.7263447 ± 0.087266	0.7638892 ± 0.082746	0.7915843 ± 0.075592	0.7545037 ± 0.073553
HCP(011)	0.0054378 ± 0.000492	0.0055432 ± 0.000460	0.0033939 ± 0.000323	0.0037810 ± 0.000340
HCP(012)	0.0003864 ± 0.000080	0.0003524 ± 0.000071	0.0003132 ± 0.000060	0.0003499 ± 0.000063
FCC(211)	0.0128840 ± 0.001583	0.0106098 ± 0.001328	0.0110364 ± 0.001216	0.0107053 ± 0.001193
FCC(100)	0.0055787 ± 0.000907	0.0074614 ± 0.000970	0.0062388 ± 0.000796	0.0057046 ± 0.000758
FCC(111)	0.0363110 ± 0.002704	0.0292115 ± 0.002242	0.0277059 ± 0.001960	0.0273772 ± 0.001942

	$9 \times 9 \times 9$	$10 \times 10 \times 10$	$11 \times 11 \times 11$	$12 \times 12 \times 12$
HCP(013)	0.196905 ± 0.021686	0.193130 ± 0.021007	0.166151 ± 0.019005	0.165818 ± 0.018732
HCP(031)	0.0019984 ± 0.000518	0.0028403 ± 0.000604	0.0021002 ± 0.000506	0.0020877 ± 0.000498
FCC(110)	0.7565756 ± 0.072684	0.7648798 ± 0.071484	0.7926171 ± 0.070978	0.7918473 ± 0.069993
HCP(011)	0.0038785 ± 0.000339	0.0038474 ± 0.000331	0.0037843 ± 0.000320	0.0031677 ± 0.000289
HCP(012)	0.0003980 ± 0.000066	0.0004467 ± 0.000069	0.0003359 ± 0.000058	0.0003732 ± 0.000060
FCC(211)	0.0106865 ± 0.001177	0.0094782 ± 0.001084	0.0096088 ± 0.001065	0.0104799 ± 0.001097
FCC(100)	0.0058812 ± 0.000760	0.0049172 ± 0.000680	0.0052633 ± 0.000686	0.0051528 ± 0.000669
FCC(111)	0.0236765 ± 0.001782	0.0204602 ± 0.001620	0.0201393 ± 0.001568	0.0210733 ± 0.001582

	$14 \times 14 \times 14$	$16 \times 16 \times 16$	$18 \times 18 \times 18$
HCP(013)	0.151283 ± 0.017382	0.180269 ± 0.018415	0.165994 ± 0.017468
HCP(031)	0.0022802 ± 0.000506	0.0013587 ± 0.000379	0.0023523 ± 0.000493
FCC(110)	0.8090616 ± 0.068734	0.7784374 ± 0.065432	0.7993910 ± 0.065548
HCP(011)	0.0028930 ± 0.000268	0.0031977 ± 0.000274	0.0028826 ± 0.000257
HCP(012)	0.0003133 ± 0.000054	0.0003542 ± 0.000055	0.0002670 ± 0.000048
FCC(211)	0.0107072 ± 0.001077	0.0091898 ± 0.000968	0.0091167 ± 0.000954
FCC(100)	0.0057119 ± 0.000685	0.0052674 ± 0.000638	0.0046035 ± 0.000590
FCC(111)	0.0177499 ± 0.001411	0.0219262 ± 0.001522	0.0153934 ± 0.001261

Appendix G

Site contribution to the total TOF (D_e = 45 kcal/mol)

	$5 \times 5 \times 5$	$6 \times 6 \times 6$	$7 \times 7 \times 7$	$8 \times 8 \times 8$
HCP(013)	0.195617 ± 0.006847	0.203907 ± 0.007066	0.208506 ± 0.005950	0.206471 ± 0.006007
HCP(031)	0.0009176 ± 0.001526	0.0011108 ± 0.001427	0.0007441 ± 0.001460	0.0008930 ± 0.001354
FCC(110)	0.7532914 ± 0.098510	0.7486553 ± 0.079320	0.7402852 ± 0.099276	0.7495540 ± 0.080509
HCP(011)	0.0049221 ± 0.000193	0.0036275 ± 0.000208	0.0053680 ± 0.000223	0.0041563 ± 0.000178
HCP(012)	0.0003886 ± 0.000101	0.0005140 ± 0.000101	0.0005576 ± 0.000101	0.0004155 ± 0.000092
FCC(211)	0.0090302 ± 0.001565	0.0103422 ± 0.001379	0.0096689 ± 0.001507	0.0094700 ± 0.001230
FCC(100)	0.0095038 ± 0.000974	0.0073156 ± 0.000932	0.0079472 ± 0.000970	0.0066393 ± 0.000890
FCC(111)	0.0263290 ± 0.001446	0.0245280 ± 0.001190	0.0269230 ± 0.001276	0.0224014 ± 0.001075

	$9 \times 9 \times 9$	$10 \times 10 \times 10$	$11 \times 11 \times 11$	$12 \times 12 \times 12$
HCP(013)	0.224232 ± 0.005060	0.221177 ± 0.004304	0.100612 ± 0.004958	0.132172 ± 0.004097
HCP(031)	0.0006306 ± 0.001339	0.0004947 ± 0.001293	0.0012609 ± 0.001222	0.0005341 ± 0.001257
FCC(110)	0.7298015 ± 0.075675	0.7374319 ± 0.069931	0.8605845 ± 0.064938	0.8307416 ± 0.056119
HCP(011)	0.0036552 ± 0.000186	0.0033840 ± 0.000179	0.0037900 ± 0.000155	0.0025970 ± 0.000126
HCP(012)	0.0004513 ± 0.000092	0.0004526 ± 0.000087	0.0001694 ± 0.000083	0.0002691 ± 0.000085
FCC(211)	0.0095294 ± 0.001217	0.0091505 ± 0.001056	0.0112254 ± 0.001064	0.0105093 ± 0.000907
FCC(100)	0.0056639 ± 0.000929	0.0062890 ± 0.000886	0.0033635 ± 0.000781	0.0069120 ± 0.000628
FCC(111)	0.0260360 ± 0.000995	0.0216204 ± 0.001007	0.0189940 ± 0.000939	0.0162648 ± 0.000967

	$14 \times 14 \times 14$	$16 \times 16 \times 16$	$18 \times 18 \times 18$
HCP(013)	0.131911 ± 0.004276	0.137868 ± 0.008381	0.165008 ± 0.008747
HCP(031)	0.0006143 ± 0.001226	0.0020876 ± 0.001293	0.0023384 ± 0.001258
FCC(110)	0.8334968 ± 0.053843	0.8200820 ± 0.068200	0.7994124 ± 0.065010
HCP(011)	0.0025240 ± 0.000109	0.0035822 ± 0.000114	0.0033473 ± 0.000115
HCP(012)	0.0002142 ± 0.000081	0.0002042 ± 0.000088	0.0002143 ± 0.000079
FCC(211)	0.0100471 ± 0.000913	0.0103432 ± 0.001190	0.0085286 ± 0.001213
FCC(100)	0.0066127 ± 0.000610	0.0081563 ± 0.000663	0.0065326 ± 0.000716
FCC(111)	0.0145803 ± 0.000921	0.0176768 ± 0.001087	0.0146183 ± 0.000959

Appendix H

Site contribution to the total TOF (D_e = 50 kcal/mol)

	$5 \times 5 \times 5$	$6 \times 6 \times 6$	$7 \times 7 \times 7$	$8 \times 8 \times 8$
HCP(013)	0.121708 ± 0.020556	0.144734 ± 0.020528	0.142933 ± 0.018677	0.096895 ± 0.014989
HCP(031)	0.0020778 ± 0.000636	0.0010560 ± 0.000415	0.0012777 ± 0.000418	0.0016735 ± 0.000467
FCC(110)	0.8004273 ± 0.090136	0.7907485 ± 0.082045	0.8027772 ± 0.075682	0.8525939 ± 0.076027
HCP(011)	0.0067171 ± 0.000539	0.0061183 ± 0.000471	0.0049787 ± 0.000389	0.0051877 ± 0.000387
HCP(012)	0.0004315 ± 0.000083	0.0005146 ± 0.000083	0.0003577 ± 0.000064	0.0002572 ± 0.000052
FCC(211)	0.0103372 ± 0.001395	0.0106768 ± 0.001299	0.0094639 ± 0.001119	0.0111358 ± 0.001184
FCC(100)	0.0026862 ± 0.000619	0.0021664 ± 0.000509	0.0024379 ± 0.000495	0.0029447 ± 0.000530
FCC(111)	0.0556150 ± 0.003293	0.0439850 ± 0.002682	0.0357736 ± 0.002214	0.0293124 ± 0.001954

	$9 \times 9 \times 9$	$10 \times 10 \times 10$	$11 \times 11 \times 11$	$12 \times 12 \times 12$
HCP(013)	0.124983 ± 0.016857	0.103752 ± 0.014697	0.089148 ± 0.012992	0.104579 ± 0.013841
HCP(031)	0.0010523 ± 0.000367	0.0011800 ± 0.000371	0.0012329 ± 0.000362	0.0008828 ± 0.000301
FCC(110)	0.8283607 ± 0.074205	0.8526161 ± 0.072042	0.8738489 ± 0.069551	0.8604012 ± 0.067885
HCP(011)	0.0050715 ± 0.000379	0.0040079 ± 0.000322	0.0035773 ± 0.000290	0.0034082 ± 0.000279
HCP(012)	0.0002585 ± 0.000052	0.0001934 ± 0.000043	0.0001819 ± 0.000040	0.0001707 ± 0.000038
FCC(211)	0.0115682 ± 0.001195	0.0120561 ± 0.001167	0.0110776 ± 0.001067	0.0109632 ± 0.001044
FCC(100)	0.0027827 ± 0.000510	0.0032928 ± 0.000531	0.0028034 ± 0.000467	0.0026611 ± 0.000448
FCC(111)	0.0259232 ± 0.001819	0.0229023 ± 0.001636	0.0181299 ± 0.001388	0.0169340 ± 0.001320

	$14 \times 14 \times 14$	$16 \times 16 \times 16$	$18 \times 18 \times 18$
HCP(013)	0.099203 ± 0.012836	0.099393 ± 0.013384	0.109745 ± 0.013483
HCP(031)	0.0009875 ± 0.000303	0.0019559 ± 0.000445	0.0017689 ± 0.000406
FCC(110)	0.8708451 ± 0.065027	0.8644926 ± 0.067491	0.8625279 ± 0.064633
HCP(011)	0.0025484 ± 0.000229	0.0033865 ± 0.000276	0.0025281 ± 0.000228
HCP(012)	0.0001661 ± 0.000036	0.0001460 ± 0.000035	0.0001414 ± 0.000033
FCC(211)	0.0108459 ± 0.000989	0.0114769 ± 0.001059	0.0098892 ± 0.000943
FCC(100)	0.0029074 ± 0.000446	0.0037446 ± 0.000527	0.0038555 ± 0.000512
FCC(111)	0.0124972 ± 0.001080	0.0154047 ± 0.001249	0.0095444 ± 0.000942